

UNIVERSIDADE FEDERAL DE MINAS GERAIS  
ESCOLA DE ENGENHARIA



DIOGO FERRAZ COSTA

Intraocular-Lens Design with Orthogonal Sinusoidal Pattern and  
Focal-Range Classification Algorithm

Belo Horizonte

2020

DIOGO FERRAZ COSTA

# Intraocular-Lens Design with Orthogonal Sinusoidal Pattern and Focal-Range Classification Algorithm

Dissertação de Mestrado apresentada à  
Universidade Federal de Minas Gerais como  
requisito parcial para obtenção do título de  
mestre em Engenharia Elétrica.

Área de concentração: Sistemas de  
Computação e Telecomunicações.

Orientador: Davies William de Lima Monteiro

Belo Horizonte

2020

C837i Costa, Diogo Ferraz.  
Intraocular-lens design with orthogonal sinusoidal pattern and focal-range classification algorithm [recurso eletrônico / Diogo Ferraz Costa. - 2020.  
1 recurso online (61 f. : il., color.) : pdf.

Orientador: Davies William de Lima Monteiro.

Dissertação (mestrado) - Universidade Federal de Minas Gerais, Escola de Engenharia.

Inclui bibliografia.  
Exigências do sistema: Adobe Acrobat Reader.

1. Engenharia elétrica - Teses. 2. Lentes intraoculares- Teses. 3. Acuidade visual - Teses. 4. Algoritmos - Teses. I. Monteiro, Davies William de Lima. II. Universidade Federal de Minas Gerais. Escola de Engenharia. III. Título.

CDU: 621.3(043)



UNIVERSIDADE FEDERAL DE MINAS GERAIS  
Escola de Engenharia  
Programa de Pós-Graduação em Engenharia Elétrica

**"Intraocular-lens Design with an Orthogonal Sinusoidal Pattern  
and Focal-range Classification Algorithm"**

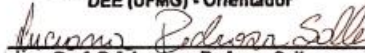
**Diogo Ferraz Costa**

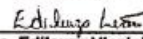
Dissertação de Mestrado submetida à Banca Examinadora designada pelo Colegiado do Programa de Pós-Graduação em Engenharia Elétrica da Escola de Engenharia da Universidade Federal de Minas Gerais, como requisito para obtenção do grau de Mestre em Engenharia Elétrica.


Aprovada em 14 de dezembro de 2020.

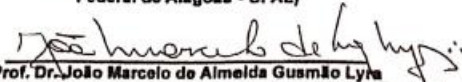
Por:

  
Prof. Dr. Davies William de Lima Monteiro  
DEE (UFMG) - Orientador

  
Prof. Dr. Luciana Pedrosa Salles  
DEE (UFMG)

  
Profa. Dra. Edileuza Virginio Leão  
Centro de Tecnologia (Universidade Estadual de Ciências da Saúde de Alagoas - UNCISAL)

  
Prof. Dr. Aydano Pamponet Machado  
Instituto de Computação (Universidade Federal de Alagoas - UFAL)

  
Prof. Dr. João Marcelo de Almeida Gusmão Lyra  
Escola de Ciências Médicas (Universidade Estadual de Ciências da Saúde de Alagoas - UNCISAL)

Dedico este trabalho aos meus pais, por terem  
construído os alicerces sobre os quais me sustento,  
emocional e profissionalmente.

## **AGRADECIMENTOS**

**Agradeço a Deus, aos amigos espirituais e aos sagrados Orixás, por iluminarem meu caminho e me sustentarem durante a árdua caminhada.**

**Agradeço à minha mãe, Sandra, por ser minha fortaleza, me dando o exemplo da humildade, perseverança, gentileza e organização (apesar de, neste último quesito eu ainda deixar bastante a desejar).**

**Agradeço ao meu falecido pai, Márcio, por ser o maior exemplo de homem que já conheci. Um grande pai, uma pessoa sensível e um amigo para todas as horas. Um grande engenheiro reconhecido mundialmente, que me estimulou a seguir o caminho da ciência (apesar de sofrido).**

**Agradeço ao meu orientador, professor, mestre e amigo, Davies, por suportar minhas ideias mirabolantes, me aconselhar em tempos de atribulações e me incentivar a sempre aprender e seguir em frente.**

**Agradeço aos integrantes do Núcleo de Fraternidade Espírita Irmã Lúcia, por terem me acolhido fraternalmente e me estimularem a seguir no caminho da caridade e do amor ao próximo.**

**Agradeço aos meus amigos das várias searas da vida, sejam dos tempos antigos ou dos novos, pois são as pessoas que conquistamos que dão sentido à nossa vida.**

“Crê em ti mesmo, age e verá os resultados.  
Quando te esforças, a vida também se esforça  
para te ajudar.”  
- Chico Xavier

## RESUMO

O setor industrial para lentes intraoculares (LIO) está constantemente procurando por novos modelos de lente para melhorar a qualidade de visão de pacientes depois de cirurgia de catarata. Esse estudo apresenta uma lente intraocular biconvexa com um padrão senoidal bidimensional refrativo distribuído sobre sua superfície posterior em uma malha ortogonal. Esse tipo de padrão permite a configuração de diferentes amplitudes e frequências das funções senoidais ortogonais, levando a diferentes desempenhos ópticos. A escolha de parâmetros permite a LIO se comportar como Monofocal, Multifocal ou Foco Estendido. A lente intraocular sob teste é modelada e inserida em um modelo de olho de Liou-Brennan modificado. Os parâmetros são sistematicamente variados e uma metodologia personalizada é empregada para verificar a classificação dada a uma lente descrita por um determinado conjunto de parâmetros. Após o algoritmo de classificação, algumas LIOs são selecionadas e têm seu desempenho avaliado através de uma análise de imagem que consiste em diferentes acuidades visuais para um objeto a uma dada distância do olho. Também, uma estimativa pré clínica da curva de defoco é simulada para essas LIOs selecionadas. Essa metodologia pode ser utilizada como uma ferramenta confiável para ajudar fabricantes de lentes na indústria a avaliar parâmetros ótimos de projeto.

**Palavras-chave:** Óptica oftálmica, Projeto de lente, Acuidade visual, Lente intraocular, Profundidade de foco, Algoritmo de classificação.



## ABSTRACT

The industrial sector for intraocular lenses (IOLs) is constantly searching for new lens models to improve vision quality of patients after cataract surgery. This study presents a biconvex intraocular lens with a bidimensional refractive sinusoidal profile distributed over its posterior surface in an orthogonal grid. This type of pattern allows the configuration of different amplitudes and frequencies of the orthogonal sinusoidal functions, leading to distinct optical performance. The choice of parameters enables the IOL to behave as Monofocal, Multifocal or Extended Depth of Focus. The intraocular lens under test is modelled and inserted into a modified Liou-Brennan eye model. The parameters are systematically varied and a custom methodology is employed to verify into which class a lens described by a certain set of parameters falls. Following the classification algorithm, some IOLs are selected to have their performance evaluated through an image analysis that consists of different visual acuities for an object at a given distance from the eye. Also, an estimated preclinical defocus curve is simulated for those selected IOLs. This methodology can be used as a reliable tool to assist lens manufacturers in industry to evaluate optimal design parameters.

**Keywords:** Ophthalmic optics, Lens design, Visual acuity, Intraocular lens, Depth of focus, Classification algorithm.

## LIST OF FIGURES

Figure 1 – Image projection of an approaching car on the retina, from the perspective of a patient with a multifocal (bifocal) IOL and another patient with a monofocal IOL [author]. .....	15
Figure 2 – Difference of strategies to keep an object in focus between a multifocal IOL (simultaneous vision) and multifocal spectacles (gaze dependent vision)[author]. .....	16
Figure 3 – Example of diffractive IOL [adapted:6].....	16
Figure 4 – Examples of conic sections (left)[8]. On the right [9], an oblate ellipsoid (blue; $k>0$ ) and a prolate ellipsoid (yellow; $-1<k<0$ ). .....	17
Figure 5 – Effect of the extended depth of focus on the projected image of the object on the retina [author]. .....	18
Figure 6 – Helmholtz-Laurance eye model schematic [12]. .....	20
Figure 7 – Gullstrand eye model schematic [12].....	20
Figure 8 – ISO eye model schematic [13]. .....	22
Figure 9 – Liou-Brennan eye model schematic [12]. .....	22
Figure 10 – Example of Snell’s Law application [author]. .....	23
Figure 11 – Example of Ray Trace report, from ZEMAX OpticStudio [author].....	24
Figure 12 – IOL design procedure [author].....	25
Figure 13 – Example of bidimensional PSF (Point-Spread Function), on the image plane (left)[author]. Associated PSF cross section (right)[author]. .....	26
Figure 14 – MTF 2D (left)[author], with the MTF curve (blue) and the diffraction limit (black); and MTF surface 3D map (right)[author].....	27
Figure 15 – Domain transformations [author].....	27
Figure 16 – Effect on the TF-MTF curve, at an arbitrary spatial frequency, of an object approaching the eye [author]. .....	28
Figure 17 – Snellen visual acuity chart [25].....	30
Figure 18 – IOL design development history [author]. .....	31
Figure 19 – Diagonal view (left), lateral view (center) and frontal view of the Periodic IOL (right)[author]. .....	32
Figure 20 – Classification algorithm [author]. .....	35
Figure 21 – Eye schematic used for unit conversion [author]. .....	39
Figure 22 – Conversion of object distance ( $S_o$ ) to depth of focus (DoF) [author]. .....	40
Figure 23 – Conversion of depth of focus to refractive power at the IOL plane [author]. .....	41
Figure 24 – Visual angle representation [author]. .....	42

Figure 25 – Conversion of normalized MTF area to preclinical logMAR score [author].....	44
Figure 26 – IOL score and classification as a function of the designed sinusoidal amplitudes and frequencies [author]. .....	46
Figure 27 – Through-Focus MTF curve for EDoF 1 [author]. .....	47
Figure 28 – Through-Focus MTF curve for EDoF 2 [author]. .....	48
Figure 29 – Through-Focus MTF curve for EDoF 3 [author]. .....	48
Figure 30 – Through-Focus MTF curve for Monofocal IOL [author]. .....	49
Figure 31 – Through-Focus MTF curve for Multifocal IOL [author]. .....	49
Figure 32 – Comparison between Symphony and AT LARA IOLs [32]. .....	50
Figure 33 – logMAR plot for pupil diameter of 3.0 mm [author]. .....	51
Figure 34 – logMAR plot for pupil diameter of 4.5 mm [author]. .....	51
Figure 35 – logMAR plot for pupil diameter of 6.0 mm [author]. .....	52

## LIST OF TABLES

Table 1 – Periodic IOL range restrictions and simulation step [author]. .....	32
Table 2 – Modified Liou-Brennan eye model specification [adapted:12].....	34
Table 3 – Image height calculations for an EFFL = 17.0118 mm [author]......	43
Table 4 – Correlation between visual acuity (Snellen) and logMAR score [author]. .....	44
Table 5 – Classification summary [author]. .....	46
Table 6 – Periodic parameters of the selected IOLs [author]. .....	46
Table 7 – Extended depth of focus IOLs TF-MTF characteristics at 50 lp/mm [author]. .....	47
Table 8 – Visual acuity of a 20/32 letter at 1 km from the eye [author]. .....	54
Table 9 – Visual Acuity of a 20/32 letter at 6 m from the eye [author]. .....	55
Table 10 – Visual Acuity of a 20/32 letter at 2 m from the eye [author]. .....	55
Table 11 – Visual Acuity of a 20/32 letter at 0.66 m from the eye [author]. .....	56

## LIST OF ABBREVIATIONS AND ACRONYMS

IOL	Intraocular lens
MIOL	Multifocal intraocular lens
DoF	Depth of Focus
EDoF	Extended depth of focus
PSF	Point-spread function
OTF	Optical transfer function
MTF	Modulation transfer function
PhTF	Phase transfer function
TF-MTF	Through-Focus Modulation Transfer Function
V.A.	Visual acuity
MAR	Minimum angle of resolution
logMAR	Logarithm of the minimum angle of resolution
EFFL	Effective Focal Length
PMMA	Polymethyl methacrylate
SIA	Surgically induced astigmatism
ANSI	American National Standards Institute
ISO	International Organization for Standardization
FFT	Fast Fourier Transform

## SUMMARY

<b>1 INTRODUCTION .....</b>	<b>12</b>
<b>2 THEORY .....</b>	<b>15</b>
2.1 Types of intraocular lenses .....	15
2.2 Types of eye models .....	19
2.3 Raytracing.....	23
2.4 Design procedure .....	24
2.5 Merit functions .....	25
2.6 Snellen eye chart.....	29
<b>3 METHODOLOGY .....</b>	<b>30</b>
3.1 Intraocular lens design.....	30
3.2 Eye model implementation .....	33
3.3 Algorithm .....	34
3.4 Units conversion .....	38
3.5 Image size calculations .....	41
3.6 Preclinical visual acuity.....	43
<b>4 RESULTS AND DISCUSSION .....</b>	<b>45</b>
4.1 3D bar chart .....	45
4.2 Visual acuity .....	50
4.3 Image simulation .....	53
<b>5 CONCLUSIONS.....</b>	<b>57</b>
<b>REFERENCES .....</b>	<b>59</b>

## 1 INTRODUCTION

In ophthalmic surgery for cataract treatment, the human crystalline is replaced by a manufactured transparent intraocular lens usually made of acrylic or silicone materials. These materials can either be rigid, such as the PMMA (polymethyl methacrylate), or foldable, such as AcrySof (Alcon Laboratories). The goal is to restore vision, since cataract causes the opacification of the crystalline lens, causing partial to total loss of vision.

The human eye also has the capacity of altering the dioptric power of the crystalline by the actuation of the ciliary muscles, that change the radius of curvature of the lens to enable the vision accommodation for different object distances. With the aging process, there is a verified loss of this accommodation process [1], in a ophthalmic disorder called presbyopia.

Usually, when inserting an intraocular lens into the eye, there is a loss of accommodation since, in the vast majority of off-the-shelf lenses, the ciliary muscles does not play a role in changing the shape of the manufactured intraocular lens. Historically, some solutions have been developed. One is the use of a monofocal intraocular lens, which usually exhibits a good contrast for distant vision, but requires the patient to wear spectacles for intermediate or near vision. Then, the multifocal intraocular lenses were implemented, which redirect, through various techniques, part of the light to different regions of the optical axis, improving the contrast of closer objects. Usually, multifocal lenses have a problem of loss of contrast for objects placed at distances other than the ones for which the additional foci have been designed. Therefore, a new class of intraocular lenses was proposed, called “extended depth of focus” (EDoF) which enables a continuous vision across different ranges of object distances, but without the low-contrast gap. It is important to note that the EDoF IOL is also called “enhanced monofocal”, such as the Vivity IOL (Alcon Laboratories) [2] or the Eyhance IOL (Johnson & Johnson) [3].

This study considers an intraocular lens design that has an orthogonal bidimensional refractive sinusoidal profile. This geometry is orthogonal and bidimensional because the sinusoidal profile is distributed across the  $x$  and  $y$  directions of the intraocular lens (which are orthogonal directions). The design is refractive because it has smooth topological surfaces that do not have any abrupt transitions causing diffraction, and is solely based on refractive effects.

It is important to notice that although IOLs with sinusoidal patterns are known in the literature, none of them uses an orthogonal sinusoidal profile. It provides a great versatility for parameter configurations, allowing the lens to perform as different classes (monofocal,

multifocal or extended depth of focus). Some IOLs with sinusoidal patterns in the literature [4] usually describe concentric radial refractive sinusoidal power variations, and not an orthogonal sinusoidal grid.

The sinusoidal profile is placed on the posterior surface of a base lens. The base lens is biconvex and symmetric, which means that the radius of curvature of the anterior surface is the same as that of the posterior surface. The sinusoidal profile can be configured with different amplitudes and frequencies, which lead to different optical performances.

The goal of this study is not only to design the specified intraocular lens, but to develop an algorithm that is capable of classifying the different sinusoidal configurations between monofocal, multifocal and extended depth of focus. After the classification is done, some of the resulting intraocular lenses are selected, with an emphasis on extended depth of focus configurations, because it reflects a market tendency since these lenses usually exhibit a continuous range of focus.

The selected intraocular lenses are analyzed in a more detailed manner. The preclinical logMAR defocus curve is simulated, as well as the image simulations for different object distances. The preclinical logMAR defocus curve provides some important pieces of information, since it exhibits the visual acuity behavior of the lens under test for different object distances. It also intrinsically considers different object spatial frequencies, not being biased towards a given frequency. The results shown by the preclinical curves are also used to compare the selected optical performances with the ANSI-standard requirements for extended depth of focus intraocular lenses. The image simulations are done after an understanding of visual angle calculations related to the Snellen chart, which is a common visual acuity test pattern used in ophthalmic practice.

The designed lenses are compared with intraocular lenses manufactured by well established brands in the ophthalmic-lens industry.

The second chapter (Theory), covers different types of intraocular lenses and eye models. Also, there is a discussion about raytracing and Snell's Law, followed by the explanation of a general IOL design procedure based on the thick lens equation. Afterwards, some important optical merit functions are explained, as well as their relation to one another. The chapter ends with an introduction to the Snellen visual acuity chart.

In the third chapter (Methodology), there is a discussion about the designed Periodic IOL used in this study, followed by the specification of a modified Liou-Brennan eye model, herein deployed. Then, the classification algorithm is explained, based on merit functions that are compared with arbitrarily preset thresholds. There are sections on unit conversions and



preclinical visual-acuity prediction, which help to evaluate the IOL behavior based on a statistical model, as well as to exhibit the results in units that are suited to clinical practice (such as additional refractive power, in diopters). There is also a section about image size calculations, which help the configuration of the adequate Snellen letter sizes via ZEMAX OpticStudio, to represent the desired situations.

In chapter four (Results and discussion), the main classification result is shown through a 3D bar chart, followed by a selection of different IOL configurations to be further analyzed. Also, the preclinical visual acuity curves are shown, followed by a comparison with the ANSI standard requirements for EDoF IOLs. The chapter ends with the results from the image simulation for different object distances.

This work is concluded with an overview of the realized developments and analysis.

## 2 THEORY

### 2.1 Types of intraocular lenses

The intraocular lenses (IOLs) can be classified according to either their number or extension of foci. A monofocal lens has a single focus, and that is often chosen to be one associated with far vision, where the object is usually further than 6 m, and the image plane then coincides with the retina. Users of this lens need spectacles for intermediate and near vision. In contrast, multifocal intraocular lenses (MIOLs) are known for having the main focus designed for objects far away from the eye, and secondary foci for intermediate (0.5-2 meter) and/or close (0.3-0.5 meter) object distances. Thus, the multifocal intraocular lenses try to partly compensate the loss of natural accommodation previously possible with the crystalline. In Figure 1, the perceived image of the car becomes blurred as it comes closer to the eye. When the car comes at certain distance equivalent to the multifocal secondary focus, the contrast of the car increases. Meanwhile the eye with a monofocal IOL still perceives it as blurred.

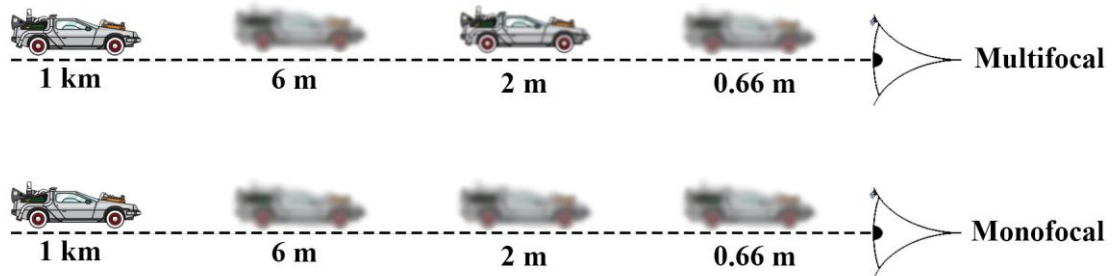


Figure 1 – Image projection of an approaching car on the retina, from the perspective of a patient with a multifocal (bifocal) IOL and another patient with a monofocal IOL [author].

The multifocality phenomena happens differently in intraocular lenses when compared to multifocal spectacles. In multifocal spectacles usually the direction of gaze is changed to obtain a different focus. In intraocular lenses, the resulting images from different foci are always overlapped, in an effect called “simultaneous vision”. Through this effect, a neuro adaptative process comes into play, called “intraocular rivalry” [5], where the brain learns how to privilege the image located on the adequate focus for a given object distance (Figure 2).

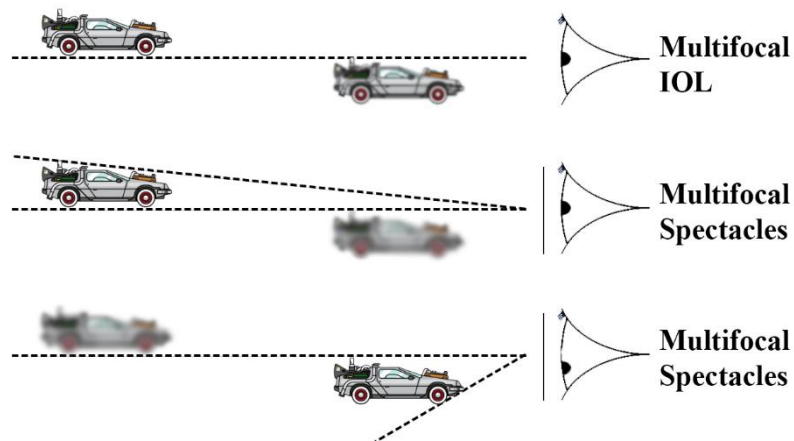


Figure 2 – Difference of strategies to keep an object in focus between a multifocal IOL (simultaneous vision) and multifocal spectacles (gaze dependent vision)[author].

Additionally, the MIOLs can be further subdivided into refractive, diffractive or hybrid. A diffractive MIOL (Figure 3) is usually made of concentric rings with a saw-tooth profile (kinoforms), designed based on diffractive principles, while a refractive lens does not have any abrupt transitions on the surface elevations and works solely on refractive phenomena.

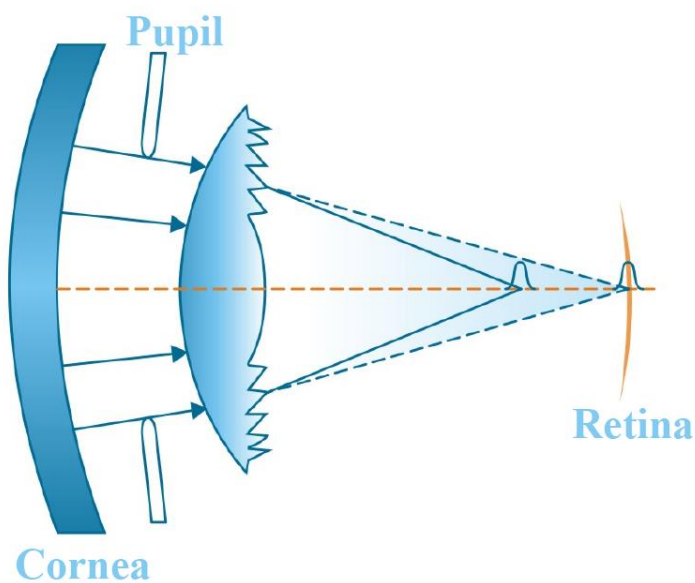


Figure 3 – Example of diffractive IOL [adapted:6].

An Extended Depth of Focus (EDoF) IOL has the characteristic of elongating the distance at which the object remains in focus, thus providing an increased range of vision. Therefore, if an EDoF IOL is designed for emmetropy (perfect vision with relaxed eye) aiming at objects 10 m distant, usually the object can be brought a few meters closer to the eye and still maintain reasonable contrast (staying in focus).

A toric IOL is mainly used to correct corneal astigmatism. This type of lens is designed by intentionally inserting a certain amount of astigmatic power to compensate for both the

naturally developed corneal astigmatism and the surgically induced astigmatism (SIA), since the incision made to access the crystalline often increases the astigmatism.

An intraocular lens can also be classified according to its asphericity. Since most of them have a curved shape, its cross section can be a sphere, a paraboloid, a hyperboloid, an oblate ellipsoid or a prolate ellipsoid (Figure 4). This classification [7] is specified by the value of the conic constant ( $k$ ) as:

$k < -1$ : Hyperbola

$k = -1$ : Parabola

$-1 < k < 0$ : Prolate ellipse

$k = 0$ : Sphere

$k > 0$ : Oblate ellipse

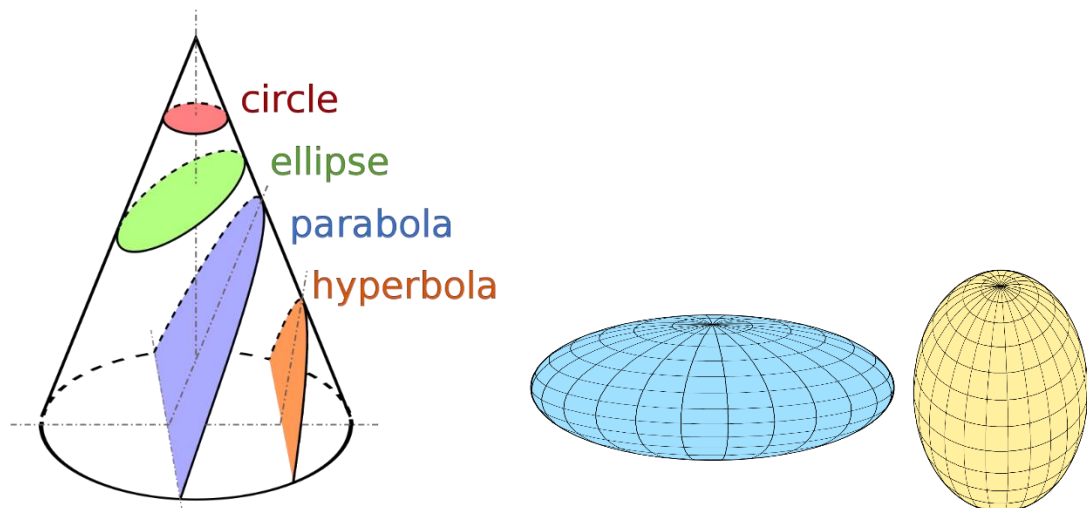


Figure 4 – Examples of conic sections (left)[8]. On the right [9], an oblate ellipsoid (blue;  $k > 0$ ) and a prolate ellipsoid (yellow;  $-1 < k < 0$ ).

Therefore, if the curvature ( $c$ ), which is the reciprocal of the radius of curvature along the axial length direction, and the conic constant are known, it is possible to specify the base geometry of an aspheric surface (Eq. 1).

$$z_{asf} = \frac{cr^2}{1 + \sqrt{1 - (1+k)c^2r^2}} \quad (1)$$

Where  $z_{asf}$  is the surface elevation in the direction along the main optical axis and  $r$  is the radial coordinate perpendicular to that axis, on the plane of the lens [7]. The complete

aspheric surface mathematical description contains other polynomial terms, but for the sake of simplicity, in this work it was modelled only with the base surface equation (Eq. 1)

In medical practice it is common to reference a given curvature as oblate or prolate. Although the terms are related to the asphericity or eccentricity (from conic surfaces in mathematics), in ophthalmology it often means a change in curvature that increases or decreases the reference refractive power.

One can also classify an intraocular lens according to its depth of focus. The depth of focus is the longitudinal distance range about the main focal plane, throughout which the image features acceptable sharpness. It is possible to convert the different values of focus shift to the equivalent field range (usually in meters from the eye) if the effective focal length of the system is known. An intraocular lens can be classified as having an Extended Depth of Focus (EDoF) if it can maintain an acceptable retinal image contrast when an object moves within a given field range. For example, if the EDoF IOL is designed to have maximum retinal contrast for distant objects, the focal plane can shift a few millimeters or fraction of millimeters off the retina and still preserve the image with a reasonable contrast. This focal plane shift can be translated to the object perspective as the object changing its position to one that the IOL had not been originally designed for. In the below example (Figure 5), a patient with an implanted EDoF IOL would perceive the image of an approaching car as gradually becoming blurred, instead of having an oscillating contrast (as it happens with some MIOLs).

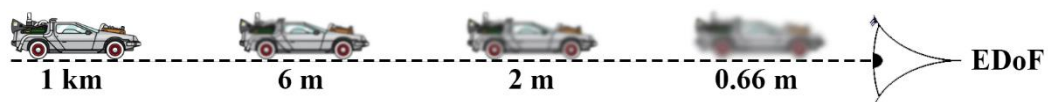


Figure 5 – Effect of the extended depth of focus on the projected image of the object on the retina [author].

According to [10], the requirements for an intraocular lens to be considered as having an extended depth of focus are the following, for a 3-mm pupil:

It must exhibit an increase of at least 0.5 D at a visual acuity of 0.2 logMAR, when compared to the reference monofocal aspheric IOL (photopic situation; monocular; distance-corrected depth of focus).

It must have at least 0.2 logMAR for an object placed at 66 cm from the eye.

The visual acuity difference from the reference monofocal aspheric IOL at 0 D must be no greater than 0.1 logMAR.

Besides, for a 4.5-mm pupil, it ought to present a better visual acuity than the reference monofocal aspheric lens too. Although the criteria specified by [10] have not been used for the classification procedure in this work, the results obtained were compared by analyzing the preclinical logMAR defocus curve. Both the classification procedure and the preclinical analysis are discussed in the Methodology chapter. The classification procedure uses the comparison between the Through-Focus MTF curve at a spatial frequency of 50 line pairs per millimeter (lp/mm) for different IOL configurations. Also, in this procedure, the curves are compared with preset thresholds that, although arbitrarily chosen, are based on the values shown in an extensive clinical trial done by Alcon about the Vivity IOL [11].

## **2.2 Types of eye models**

The interest in the physiological aspects and optical properties of the human in vivo eye, and how they relate to visual acuity, come from very ancient times. Historically, after Gauss (1841) established the basic laws that govern image formation properties, many theoretical models have been proposed. These proposed eyes hereby mentioned, consider strictly optical characteristics and there is no attempt to predict neurovisual effects. Another important aspect is that the IOL is often designed for a specific distance inside the capsular bag, but surgery its longitudinal position may incidently be different, influencing the quality of the projected image. Also, the placement of the IOL can exhibit a decentration from the main optical axis, or be tilted to one direction, which may also affect performance. Even further, rotation about the optical axis can happen, as a especially detrimental feature in the case of asymmetric lenses, as the toric IOL.

In the late 19<sup>th</sup> century, Helmholtz undertook a very thorough study on this subject, and published the now famous collection Helmholtz Treatise on Physiological Optics. This model was later modified by Laurance and became known as the Helmholtz-Laurance model (Figure 6), which contains all optical surfaces found in the biological eye. Although this model designates refractive indices to eye components that not necessarily correspond to true measured values, its overall properties have a close resemblance to those of the human eye [12].

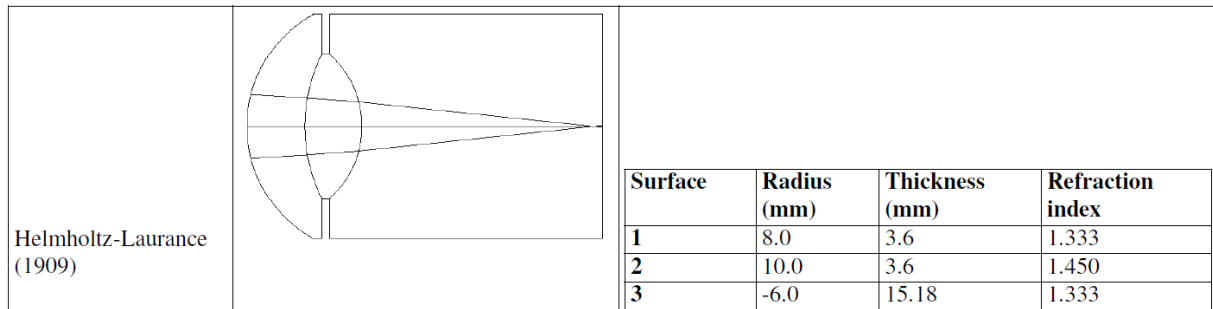


Figure 6 – Helmholtz-Laurance eye model schematic [12].

Afterwards, the Swedish Ophthalmologist Allvar Gullstrand (1862-1930) conducted important research in the field of physiology and in 1911 received the Nobel Prize for his work regarding the eye as an optical element. While Gullstrand's simplified schematic eye treats the cornea as a single refracting surface, just as the previous model from Helmholtz-Laurence, in Gullstrand's non-simplified model the cornea is considered to have two surfaces, which guarantees a perfect image formation at the retina. Although it simplifies the cornea, the vitreous and the aqueous humor, this model is especially suitable for the computation of intraocular lens (IOL) power, as it also contains the anterior and posterior surface of the crystalline lens. One of the simplest eye models available is the Emsley schematic eye, since it contains just a single refractive surface. Due to its simplicity, it is widely used in undergraduate courses in optometry, ophthalmology and vision science [12].

Gullstrand's classic eye model (Figure 7) has all surfaces spherical. However, already Helmholtz [13] had measured the cornea and described it as a prolate conicoid of rotation, which was well known to Gullstrand. To take the effect of the spherical aberration of the cornea into account, the axial length of his model is such that paraxial focus falls on the retina.

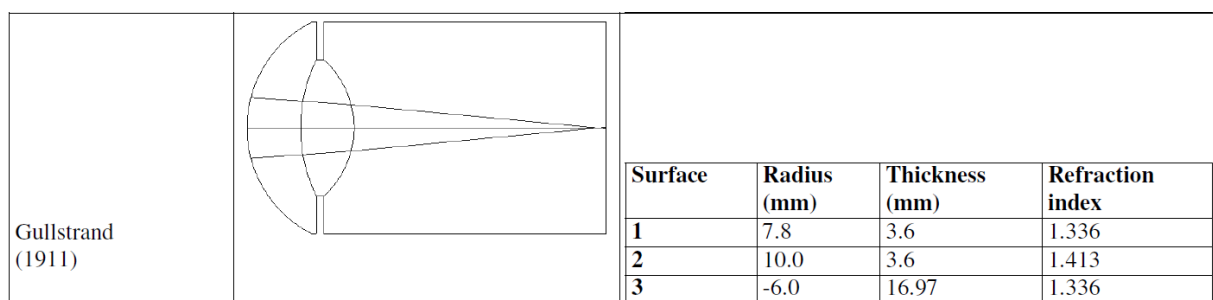


Figure 7 – Gullstrand eye model schematic [12].

Lotmar [13] was the first to introduce aspherical surfaces in an eye model. The anterior corneal surface was given a shape in accordance with measurements by Bonnet. The posterior lens surface was arbitrarily given a parabolic shape, while other surfaces remained spherical. The lens was treated as homogeneous, i.e., without a gradient index. Lotmar's aspheric eye

model is paraxially emmetropic. For principal rays at finite angles to the optical axis he calculated spherical aberration and found it to be largely in agreement with the experimental findings available to him.

Atchison [14] developed three-surface paraxial schematic emmetropic eye models based on data for 106 healthy emmetropic eyes of Caucasian subjects aged from 18 to 69 years. It is a statistical model that tries to incorporate aging effects in myopia. With increase in age in his adult schematic emmetropic eye models, anterior chamber and vitreous chamber depths, anterior lens radius of curvature, and lens equivalent power all decreased, while lens thickness and axial length increased [15].

The ISO eye model (Figure 8) is one of the most common when reporting IOL performance results. This happens not because of its accuracy, or representation of the human eye, but because it is used as a device in laboratory where one can physically insert the manufactured IOL and test the prototype in an optronic setup. An intraocular lens designed to have a good performance in an eye with typical biometric characteristics can show an inferior performance in the ISO eye than in a more accurate model, such as the Liou & Brennan. The ISO model eye proposed in ISO 11979-2 is specifically designed to test the behavior of IOLs and for IOL comparison purposes. It is not designed to provide a very similar appearance of the human eye anatomy, nor to provide a good similarity to the optical behavior of the human eye. The ISO model cornea must be free of aberrations (color and spherical), and it is usually implemented as an achromatic doublet that meets both requirements. Note, however, that this is a big difference to a real human cornea, which has an average amount of spherical aberration (in Zernike notation,  $Z_{(4,0)}$ ) of  $Z_{(4,0)}=+0.27 \mu\text{m}$  for a 6-mm entrance pupil diameter (at the anterior cornea side). The IOL under test is placed in a liquid chamber filled with liquid, which is very similar to the medium inside the human eye. In fact, a physiological water-salt solution (with a mass ratio of 0.9%) is used as a medium, usually called serum. The cornea and the fluid cavity are separated by an air gap. For most ISO tests, the convergent rays from the cornea are required to hit a point with a diameter of 3 mm on the tested IOL, usually with a 3-mm aperture (aperture stop) directly in front of the IOL. Please note that the corresponding aperture (greater than 3 mm) can also be used in front of the cornea (entrance pupil) to meet the requirements [16].



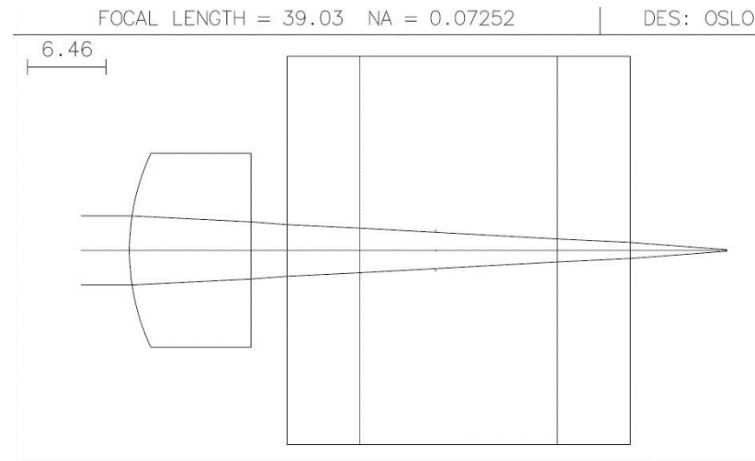


Figure 8 – ISO eye model schematic [13].

In 1997 Liou & Brennan [17] have proposed an interesting model (Figure 9), which is, according to [12], the closest to anatomical, biometric and optical data as compared to the physiological eye. Their objective was to develop a model that could be used to predict visual performance under normal and altered conditions of the eye, using empirical values of ocular parameters. In the Liou & Brennan eye there is model for the human crystalline, using a GRIN (Gradient Index) surface. In this study, the crystalline model is replaced with the designed intraocular lens parameters, with a different geometry and a fixed refractive index. In this eye, the cornea is also modelled with different curvatures and conic constants on both the anterior and posterior surfaces.

Surface	Radius (mm)	Thickness (mm)	Asphericity	Refraction index (555nm)
1	7.77	0.50	-0.18	1.376
2	6.40	3.16	-0.60	1.336
3	12.40	1.59	-0.94	Grad A
4	Infinity	2.43	—	Grad P
5	-8.10	16.27	0.96	1.336

$GradA = 1.368 + 0.049057 \cdot z - 0.015427 \cdot z^2 - 0.001978 \cdot r^2$      $GradP = 1.407 - 0.006605 \cdot z^2 - 0.001978 \cdot r^2$   
 $n(\lambda) = n(0.555\mu m) + 0.0512 - 0.1455 \cdot \lambda + 0.0961 \cdot \lambda^2$

Figure 9 – Liou-Brennan eye model schematic [12].

All of the models above have their own merit on describing the optical and physiological properties of the human eye. Depending upon the application/research that will be implemented, one or other eye should have more desirable features than the other, varying from an extremely

simple and approximate eye model to more sophisticated and anatomically correct ones. In this study, a modified version of the Liou & Brennan eye model was implemented, as further discussed in the Methodology.

### 2.3 Raytracing

The raytracing procedure is of vital importance for any geometrical optics simulation. Basically, it is a procedure realized upon each of the simulated rays from the source object to the image plane (retina). As the rays cross different surfaces of the optical system, they suffer refraction according to Snell's Law (Eq. 2).

$$n_1 \sin \theta_1 = n_2 \sin \theta_2 \quad (2)$$

Where  $n_1$  and  $n_2$  are refractive indices of the incident and transmitted planes respectively and  $\theta_1$  and  $\theta_2$  are the angles of incidence and refraction. This means that when a light ray reaches the interface that separates the original medium from another material medium, it is deflected to a direction that is closer or further from the normal vector, depending on the relation between the refractive indices of both materials. On the left side of Figure 10, the incident light ray traverses from a medium with a lower refraction index to a medium with a higher refraction index. On the right side of the same figure, the incident light ray traverses from a medium with a higher refraction index to a medium with a lower refraction index (the opposite scenario).

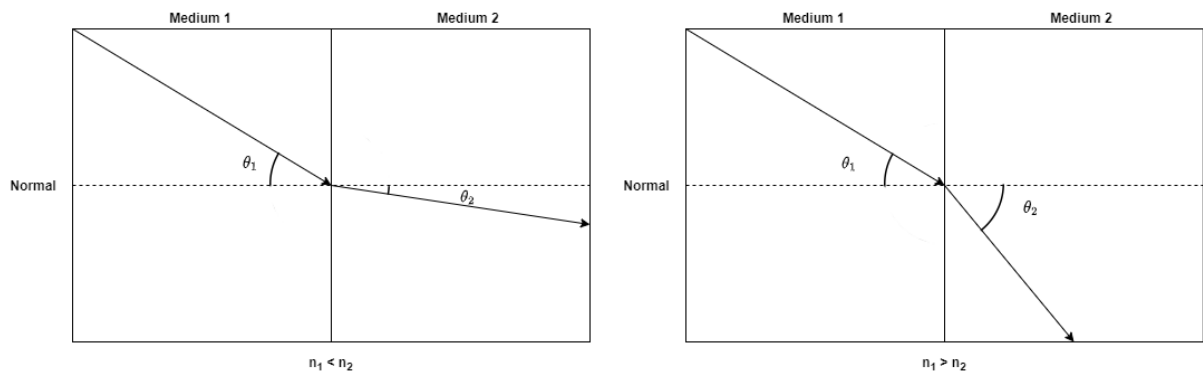


Figure 10 – Example of Snell's Law application [author].

It is possible to check the raytracing results in the ZEMAX OpticStudio software [18] (Figure 11). It shows the chief ray results crossing each surface. The first three columns specify the spatial position of the ray incidence ( $x$ ,  $y$ ,  $z$  positions). The following three columns show

the cosine of the incidence angle in the same directions. Then, ZEMAX internally calculates the surface normal vector and applies the Snell's Law to simulate the ray deflection.

Real Ray Trace Data:												
Surf	X-coordinate	Y-coordinate	Z-coordinate	X-cosine	Y-cosine	Z-cosine	X-nrcnal	Y-nrcnal	Z-nrcnal	Angle in	Path length	Comment
OBJ	-0.000000000E+000	-0.000000000E+000	0.000000000E+000	-0.0000016739	0.000002952	1.000000000	-	-	-	0.000000000	0.000000000	Objeto
1	-1.873917403E+000	2.951589171E-001	0.000000000E+000	-0.0000016739	0.000002952	1.000000000	0.000000000	0.000000000	-1.000000000	0.000000000	1.000000000E+006	Referencia
2	-1.6739260874E+000	2.951583292E-001	1.877773790E-001	0.0598540933	-0.0105186262	0.9981636878	-0.2145125884	0.0378243570	-0.975985591	12.58125815	5.187773790E+000	Cornea Anterior
3	-1.6421941245E+000	2.895631170E-001	2.187332851E-001	0.0537554164	-0.0094795303	0.9985091450	-0.2515214533	0.0443500184	-0.9668350606	11.324460995	5.3193270063E-001	Cornea Posterior
4	-1.4838490378E+000	2.6154262066E-001	0.000000000E+000	0.0537554164	-0.0094785303	0.9985091450	0.000000000	0.000000000	-1.000000000	3.129026941	2.9456582642E+000	Pupila (vignettes)
5	-1.4838490378E+000	2.6154262066E-001	0.000000000E+000	0.0537554164	-0.0094785303	0.9985091450	0.000000000	0.000000000	-1.000000000	3.129026941	0.000000000E+000	SC Inicio
6	-1.48007464481E+000	2.6097709393E-001	7.0199448394E-002	0.0577272841	-0.0101708777	0.9982904972	-0.0916815150	0.0161659247	-0.9956571512	2.212707383	7.0214127476E-002	LIO Anterior
7	-1.3957890965E+000	2.4611527709E-001	-6.2336748919E-002	0.0746860089	-0.0131691584	0.9971201399	0.084605438	-0.0152453266	-0.9961386221	8.397209611	1.4600643875E+000	LIO Posterior
8	-1.2855085484E+000	2.2666984102E-001	0.000000000E+000	0.0746860089	-0.0131691584	0.9971201399	0.000000000	0.000000000	-1.000000000	4.349382555	1.4765891190E+000	SC Fin
9	9.5421098557E-003	-1.6025314204E-003	0.000000000E+000	0.0997805079	-0.0175939597	0.9948539097	0.000000000	0.000000000	-1.000000000	4.349382555	1.7393936592E+001	Imagen

Paraxial Ray Trace Data:											
Surf	X-coordinate	Y-coordinate	Z-coordinate	X-cosine	Y-cosine	Z-cosine	Comment				
OBJ	-0.000000000E+000	-0.000000000E+000	0.000000000E+000	-0.0000016739	0.000002952	1.000000000	Objeto				
1	-1.873917403E+000	2.951589171E-001	0.000000000E+000	-0.0000016739	0.000002952	1.000000000	Referencia				
2	-1.67392608731E+000	2.951582750E-001	0.000000000E+000	0.0587626134	-0.0103614342	0.9982182106	Cornea Anterior				
3	-1.6444920216E+000	2.8996831297E-001	0.000000000E+000	0.0528605195	-0.0093207358	0.998584056	Cornea Posterior				
4	-1.4772116295E+000	2.6047226650E-001	0.000000000E+000	0.0528605195	-0.0093207358	0.998584056	Pupila				
5	-1.4772116295E+000	2.6047226650E-001	0.000000000E+000	0.0528605195	-0.0093207358	0.998584056	SC Inicio				
6	-1.4772116295E+000	2.6047226650E-001	0.000000000E+000	0.0587425597	-0.0100284665	0.9983309814	LIO Anterior				
7	-1.3901529616E+000	2.4512147796E-001	-6.1833375133E-002	0.0736900704	-0.0129935476	0.9971965409	LIO Posterior				
8	-1.2813885599E+000	2.2594337588E-001	0.000000000E+000	0.0736900704	-0.0129935476	0.9971965409	SC Fin				
9	-3.7053099609E-003	6.5334611799E-004	0.000000000E+000	0.0962343166	-0.0173213604	0.9950125575	Imagen				

Figure 11 – Example of Ray Trace report, from ZEMAX OpticStudio [author].

## 2.4 Design procedure

In order to successfully design an intraocular lens, it is necessary to understand two equations: thick and thin lens equations. They are the starting point when one wishes to design an intraocular lens with a desired refractive power, since it converts the geometric specifications of an intraocular lens (curvature, medium, lens thickness) into refractive power.

The thick lens equation (lensmaker equation) predicts the refractive power of a lens immersed in air, in which the thickness is not negligible (finite thickness). Instead the refraction must depend on the thickness of the lens (Eq. 3).

$$P = \frac{1}{f} = (n_{IOL} - 1) \left[ \frac{1}{R_1} - \frac{1}{R_2} + \frac{(n_{IOL}-1)d}{n_{IOL}R_1R_2} \right] \quad (3)$$

Where  $P$  is the refractive power in diopters,  $f$  is the focus,  $R_1$  is the radius of curvature of the IOL anterior surface,  $R_2$  is the radius of curvature of the IOL posterior surface,  $n_{IOL}$  is the refraction index of the IOL material and  $d$  is the lens thickness.

The thin lens equation is a simplification of the thick lens equation, where the lens thickness  $d$  is very small when compared with the curvatures of the surfaces of the lens [19]. Since in this study, the modelled IOL has a finite thickness that is not negligible, the thin lens equation was not used.

When designing an intraocular lens, usually the starting point is the choice of the base dioptic power, for example, 20 D. Also, the material that the lens will be manufactured is extremely important. These choices act as a restriction on the possible values of radii of

curvature and lens thickness present in the design. The thick lens equation can be further simplified depending on the design preferences. For instance, if a symmetrical biconvex IOL is desired, the modulus of  $R_1$  equals that of  $R_2$ . If a more general biconvex IOL is wanted, the curvatures can assume different values. By convention,  $R_1$  is positive and  $R_2$  is negative. If any surface is planar, the radius of curvature is infinite. One can also design the lens thickness not only according to the desired optical performance, but taking into account the mass of the material and its effects when implanted in the capsular bag through surgery.

Therefore, the general design procedure is specified in Figure 12:

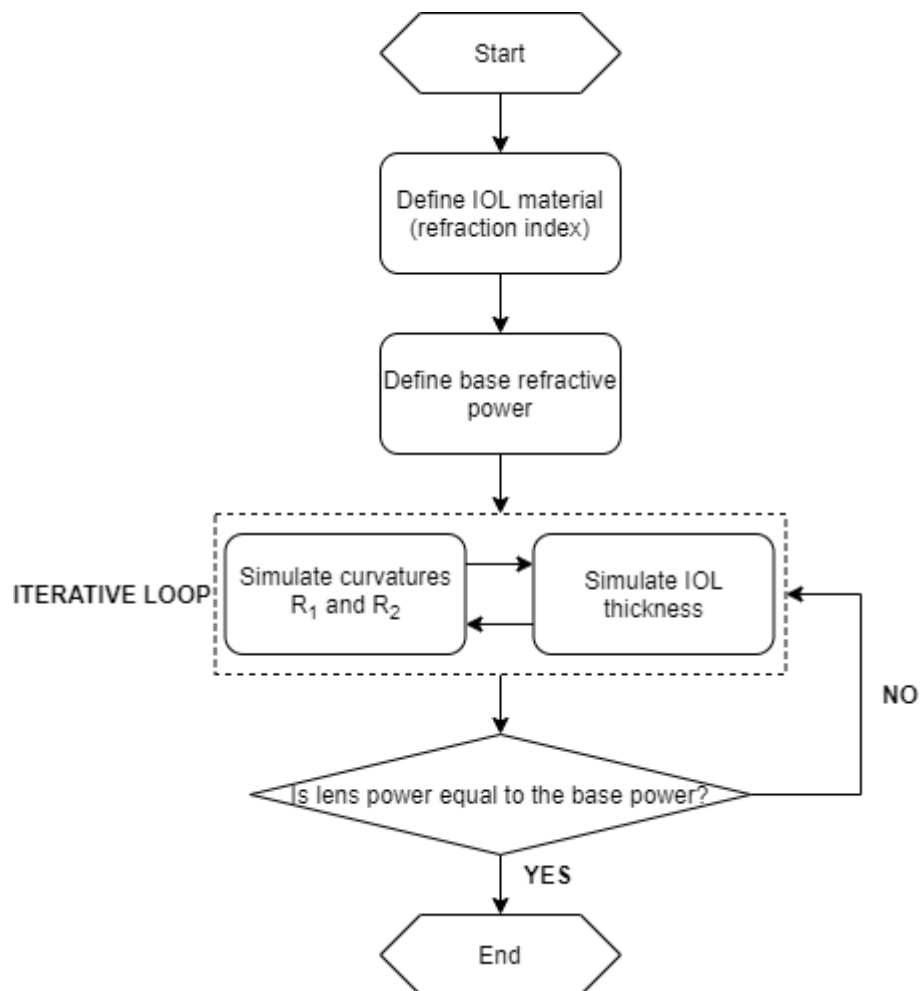


Figure 12 – IOL design procedure [author].

## 2.5 Merit functions

For the purpose of lens performance evaluation, two types of curves were computed: the Modulation Transfer Function (MTF) [20] and the Through Focus Modulation Transfer Function (TF-MTF).

To understand the Modulation transfer function, first one must understand the Point-Spread Function (PSF). The PSF (Figure 13) exhibits the response of an optical imaging system to a point source or point object. In practical systems, even if the source is infinitesimally punctual, the image is not. This is intrinsically a result of diffraction, due the effects of a finite aperture. Moreover, the system aberrations will spread the point further. The PSF is known as the impulse response of an optical system.

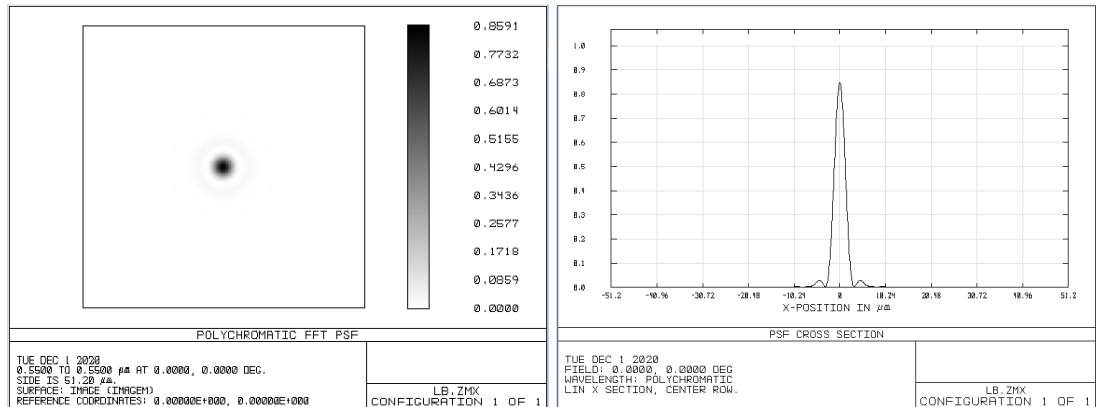


Figure 13 – Example of bidimensional PSF (Point-Spread Function), on the image plane (left)[author].  
Associated PSF cross section (right)[author].

The Optical Transfer Function (OTF) is the Fourier transform of the PSF and will usually have both real and imaginary components. The Modulation Transfer Function (or MTF) is defined as the modulus (or magnitude) of the OTF. The angular component of the OTF is denominated Phase Transfer Function (PhTF).

An ideal optical system would image an object point perfectly as a point. However, due to the wave nature of radiation, diffraction occurs, caused by the limiting edges of the aperture stop of the system. The result is that the image of a point is a blur, no matter how well the lens is corrected. The aperture also has a relation with contrast: when the aperture increases, the contrast increases as long as the “clear optical zone” is aberration-free. When the aperture decreases, the contrast also decreases but the depth of focus increases. In ophthalmic optics, the aperture is the pupil which frequently changes its diameter based on the intensity of the light [21]. Therefore, the diffraction limit changes its value during the natural course of the day, but it also means it is associated with the best contrast with which the image can be resolved.

On the left side of Figure 14, it is possible to see an example of 2D MTF curve (blue line), up to a spatial frequency of 50 lp/mm and the corresponding diffraction limit of the system (black line). On the right side of the same figure, it is possible to see the 3D MTF surface map, which contains the MTF information for all rotation angles.

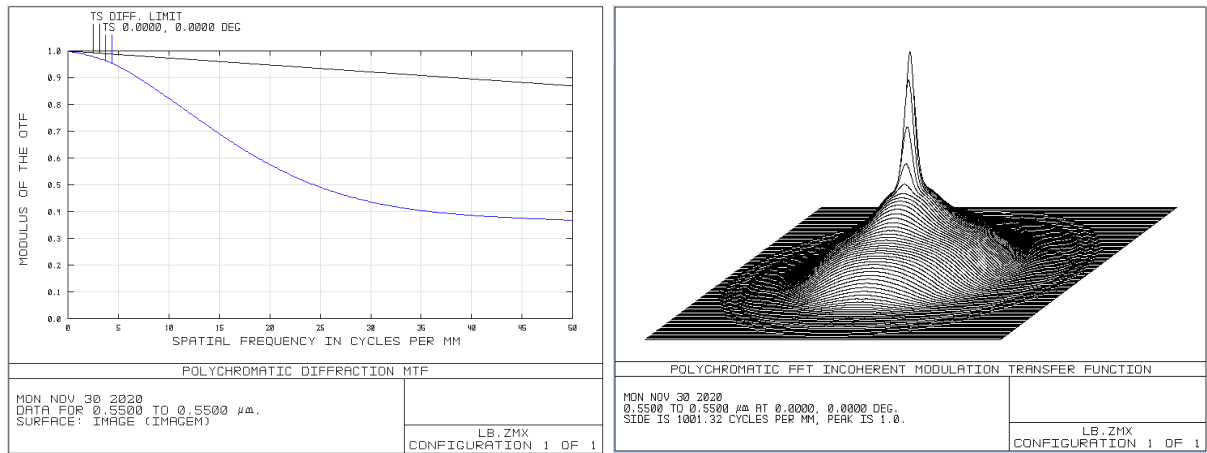


Figure 14 – MTF 2D (left)[author], with the MTF curve (blue) and the diffraction limit (black); and MTF surface 3D map (right)[author].

Since the MTF is modulus of the OTF, it represents the system frequency response, i.e. it converts the PSF information in the spatial domain to the MTF frequency domain. This mathematical operation converts bidimensional spatial information ( $x$  and  $y$  positions) into spatial frequency (cycles per millimeter; equivalent to line pairs per millimeter). The MTF curve is very important in visual acuity measurements because it does not depend on the object distance per se, but depends on the frequency contents exhibited by that object on a given distance. For example, a large object that is located further from the eye can exhibit the same spatial frequency contents when compared to a smaller object located closer to the eye. In Figure 15 it is possible to see the Fourier and Inverse Fourier transforms applied to the PSF and OTF respectively. Also, the OTF can be further divided into the MTF and the PhTF.

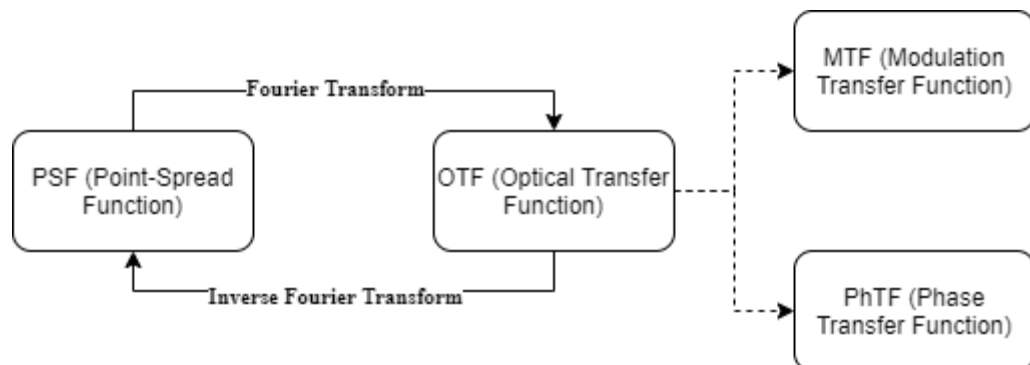


Figure 15 – Domain transformations [author].

In ophthalmic optics, the MTF is usually reported up to a spatial frequency of 100 lp/mm, since it is related to a PSF that is compatible with typical dimensions of photoreceptors [22] and for being a frequency that the reference human eye, with good visual

acuity, can typically still perceive on a usual Snellen chart. For a typical photoreceptor diameter of 4  $\mu\text{m}$ , the maximum spatial frequency that the image can be accurately represented on the retinal plane is equal to 125 lp/mm. This corresponds roughly to a visual acuity of 20/6.5 for an object at 6 m from an eye with an effective focal length of 17 mm.

The Through Focus Modulation Transfer Function (TF-MTF) gives information that is complementary to the MTF. It describes how the MTF of an optical system, at a certain spatial frequency, varies as the image plane moves through the focal plane. For example, a monofocal aspheric intraocular lens is often designed to have an optimal contrast when an object is placed at a certain distance from the eye (associated with the called “distant focus”). This scenario is represented by the blue curve (Figure 16). In this case, two points of the TF-MTF curve were arbitrarily selected, one representing the contrast peak at the retinal plane (focus shift of 0 mm) and other representing a low contrast zone in a region anterior to the retinal plane (focus shift of  $\sim -0.18$  mm). As the object comes closer to the eye, the entire curve is displaced to the right (represented by the purple curve), in a region behind the eye. When this happens, the contrast that is present on the retinal plane is no longer the main peak, but the low contrast valley. This causes the object to be perceived as blurred, as long as the spatial frequency of the object spectrum is 50 lp/mm on the retinal plane (which is the case for this particular analysis).

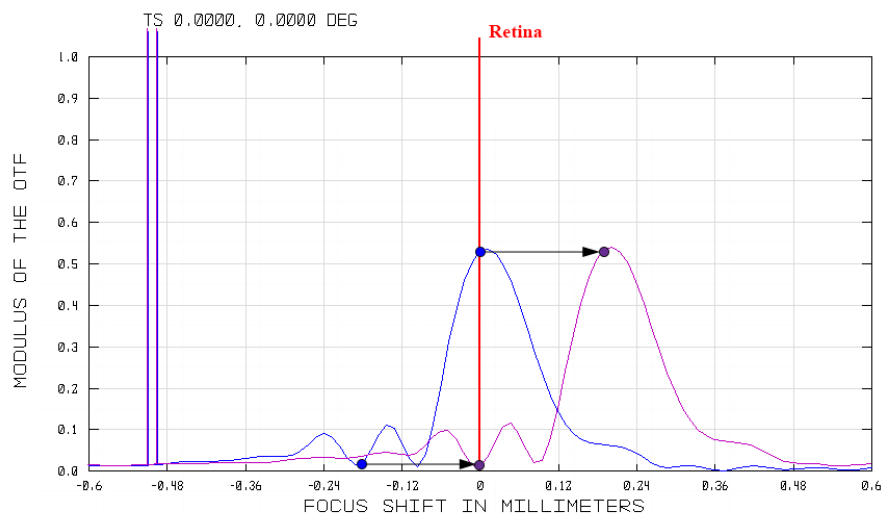


Figure 16 – Effect on the TF-MTF curve, at an arbitrary spatial frequency, of an object approaching the eye [author].

In ophthalmic optics, it is common to evaluate the TF-MTF at a frequency of 50 cycles per millimeter, since it corresponds to the fundamental frequency of the 20/40 line on the Snellen eye chart, which is an acceptable value for visual acuity [22].

Another important parameter in optics is the Strehl ratio. The Strehl ratio of the imaging system is given by the ratio of the central peak of its aberrated and diffraction-limited point-spread functions (PSF) [23].

## **2.6 Snellen eye chart**

First introduced by Dutch ophthalmologist Dr. Hermann Snellen in 1862, the Snellen chart is the current standard for measurement of visual acuity in clinical practice because it is readily available as well as quick and easy to perform. The chart has letters of different sizes arranged from largest at the top to smallest at the bottom, which are read, one eye at a time, at a distance of 6 m (20 ft). Each letter on the chart subtends an angle of 5 minutes (min) of arc at the appropriate testing distance, and each letter part subtends an angle of 1 min of arc. Accepted convention does not specify Snellen acuity in angular terms. Instead, Snellen acuities are usually expressed as a fraction with the numerator equal to the distance from the chart and the denominator being the size of the smallest line that can be read. The reciprocal of the fraction equals the angle, in minutes of arc, that the stroke of the letter subtends on the patient's eye and is called the minimum angle of resolution (MAR) [24]. An example of the Snellen visual acuity chart is shown in Figure 17.



<b>E</b>	1	20/200
<b>F P</b>	2	20/100
<b>T O Z</b>	3	20/70
<b>L P E D</b>	4	20/50
<b>P E C F D</b>	5	20/40
<b>E D F C Z P</b>	6	20/30
<hr style="border: 2px solid green;"/>		
<b>F E L O P Z D</b>	7	20/25
<b>D E F P O T E C</b>	8	20/20
<hr style="border: 2px solid red;"/>		
<b>L E F O D P C T</b>	9	
<b>F D P L T C E O</b>	10	
<b>P E Z O L C F T D</b>	11	

*Figure 17 – Snellen visual acuity chart [25].*

### 3 METHODOLOGY

#### 3.1 Intraocular lens design

Initially, the base lens design was thought of as being a plane-convex intraocular lens, where the posterior planar surface was modified to include the orthogonal bidimensional sinusoidal characteristics. However, with this approach, it was hard to focus the light rays on the optical axis to correct for base defocus. Therefore, the base design was changed to a biconvex symmetrical structure (Figure 18).

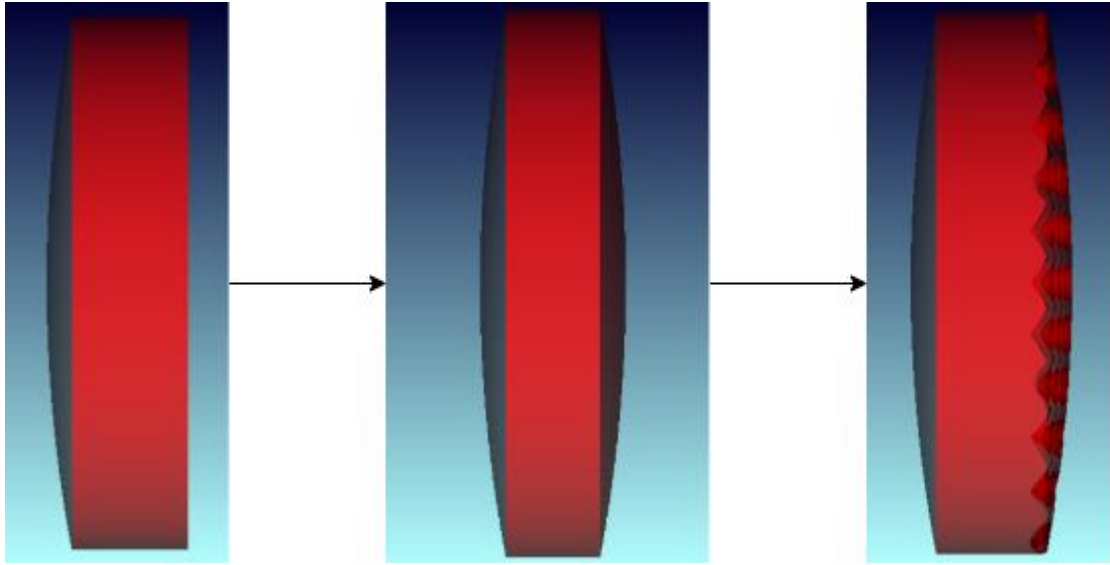


Figure 18 – IOL design development history [author].

In this study, the optical system was modelled using ZEMAX OpticStudio. Both the base Standard lenses designed for this study are biconvex with their main focus designed for maximum contrast of infinitely distant objects.

The intraocular lens herein proposed features a sinusoidal surface distributed over the posterior surface with an aspheric base curve and is referred to as Periodic. This design was chosen in this work because it is possible to alter the sinusoidal amplitude and frequency, increasing the number of design parameters. With this increase and the first simulation results, it was possible to observe that depending on the configuration, the designed lens can behave according to different IOL classes [26,27].

The equation that describes this compound surface is shown in (Eqs. 4 and 5). The base parameters of the previously designed Standard surface were maintained and only the Periodic parameters have been varied before the classification methodology was applied.

$$z_{asf} = \frac{cr^2}{1 + \sqrt{1 - (1+k)c^2r^2}} \quad (4)$$

$$z_{per} = z_{asf} - A \left\{ \frac{1}{4} [1 + \cos(2\pi\alpha x)][1 + \cos(2\pi\beta y)] - 1 \right\} \quad (5)$$

Where  $z_{per}$  is the elevation in the direction along the main optical axis,  $\alpha$  is the frequency of peaks along the  $x$  axis and  $\beta$  is the frequency along the  $y$  axis, both in cycles/mm. Its back

view profile is shown in Figure 19, with an exceptionally large wave amplitude for the sake of more clearly illustrating its intended shape.

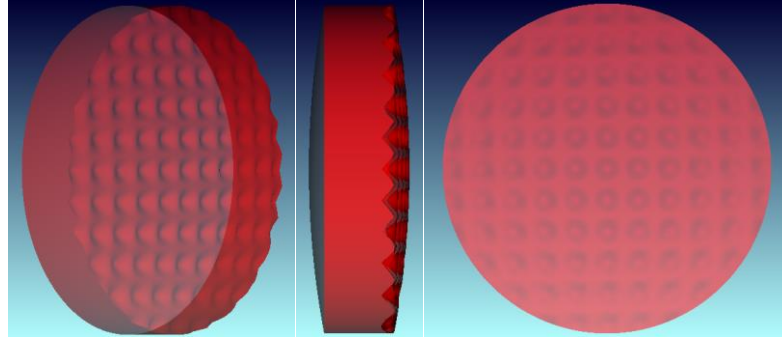


Figure 19 – Diagonal view (left), lateral view (center) and frontal view of the Periodic IOL (right)[author].

Two types of base biconvex IOLs were generated, one aspheric and one spherical. The curvature of the aspheric IOL and the conic constants were optimized for emmetropia with a pupil of 6.0 mm of diameter. The spherical IOL was optimized for emmetropia with a pupil of 3.0 mm of diameter.

The Periodic surface replaces the posterior surface of the base spherical IOL. The Periodic surface allows the configuration of a different sinusoidal frequency along the  $x$  and  $y$  axes. In this study, the frequencies in both directions are always equal. The results are for monochromatic light with a wavelength of 550 nm (green).

The amplitude ( $A$ ) and frequency ( $f$ ) were configured in a range according to Table 1. There was a total of 40 simulated IOLs, in which the minimum and maximum amplitudes and frequencies were chosen as to maintain at least a MTF of 0.43 at 100 lp/mm. This is the specified minimum contrast of a Monofocal IOL in accordance to the ISO standard [28].

Table 1 – Periodic IOL range restrictions and simulation step [author].

	Minimum	Maximum	Step
Amplitude (mm)	0.25E-3	1.25E-3	0.25E-3
Frequency (cycles/mm)	0.25	2.00	0.25

Since the proposed IOL design is entirely refractive, it is expected that it will exhibit reduced negative dysphotopic phenomena, such as halo and glare. The halo effect usually consists of a ring of light around a given point object, and glare distorts a given point object in a star burst fashion. Both effects are highly associated with diffractive IOLs, since the light diffraction can generate interference patterns and wavefront distortions that lead to such optical conditions. Halo, nevertheless, can also be experienced with refractive multifocal lenses due to the superimposed images from different foci.

### **3.2 Eye model implementation**

The eye model used to simulate an optical system similar to the human eye was a modified Liou-Brennan eye model. The first optical element in this model is a lens emulating a cornea of 0.5 mm of central thickness. It has most of the refractive power of the eye, i.e. around 40 D. After the cornea, the model specifies the anterior chamber, which is filled by an aqueous material with refractive index of 1.336 and a depth of 3.16 mm along the main optical axis. Then, it reaches the pupil that is emulated by an optical clear aperture of a given diameter. In this study the aperture was set to 3.0 mm of diameter. In this study, the original Liou-Brennan crystalline lens was replaced by a custom designed intraocular lens with around 20 D.

The Liou-Brennan eye model features an axial length of 23.95 mm, which means the distance between the first surface (front cornea) and the image plane (retina). Therefore, the sum of all distances and thicknesses from the front cornea to the retina must be equal to the specified axial length. To account for this fixed figure, the distance between the back IOL and the image plane (vitreous cavity) has 18.70 mm. The vitreous cavity contains a transparent, gelatinous substance, called vitreous humor, that in the Liou-Brennan eye is modelled as having 1.336 of refractive index for a 550 nm light.

The modified Liou-Brennan eye model has the parameters shown in Table 2.

Table 2 – Modified Liou-Brennan eye model specification [adapted:12].

	Anterior Radius (mm)	Posterior Radius (mm)	Anterior conic	Posterior conic	Central Thickness (mm)	Refractive index (555 nm)
Cornea	7.770	6.400	-0.180	-0.600	0.50	1.376
Anterior Chamber	-	-	-	-	3.16	1.336
Aspheric IOL	15.607	-15.607	-10.255	-18.010	1.59	1.492
Spherical IOL	16.145	-16.145	0	0	1.59	1.492
Posterior Chamber	-	-	-	-	18.70	1.336

### 3.3 Algorithm

An algorithm was developed with Python programming language to enable the simulation of different IOL parameters (Figure 20). This approach greatly increases the efficiency of evaluating a large number of topologies. This classification algorithm was proposed and implemented because it better systematizes the process of decision-making on a large number of intraocular lenses classes, allowing the analysis of many configurations that lead to different optical behaviors. Although the classification algorithm includes the Monofocal, Multifocal and Extended Depth of Focus (EDoF) classes, the main goal is to find as many EDoF IOLs as possible, since it represents a development trend in the field of study to propose lenses that have a continuous range of vision, possibly reducing the need for correcting spectacles after surgery.

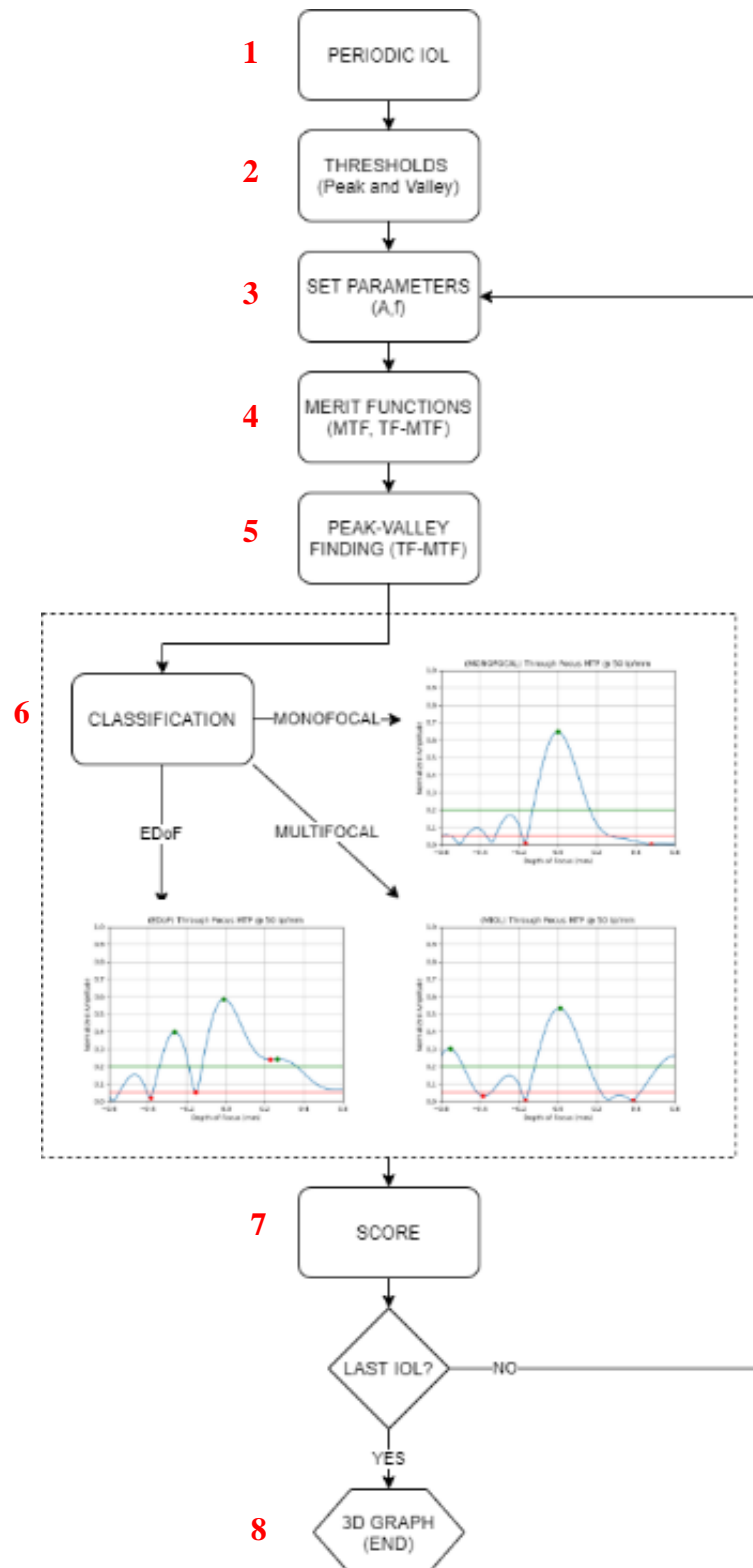


Figure 20 – Classification algorithm [author].

The first step in the algorithm (Figure 20) is to specify the base lens parameters for the Periodic IOL (step 1). Then, two types of thresholds are arbitrarily set, the peak and valley thresholds (step 2). They are input parameters used by the algorithm to aid in the classification process and will be further discussed. The next step is to modify the frequencies ( $f$ ) and

amplitudes ( $A$ ) of the IOL Periodic surface (step 3) in a given parameter range. This range selection in which the amplitudes and frequencies vary are further discussed in section 4.1. In step 4, the merit functions (MTF and TF-MTF) are extracted from each individual configuration and saved in the database. In each TF-MTF curve a Peak Detection Function (PDF) is executed, where all the peaks are found (step 5). The valleys are found by applying the same function but on the inverted TF-MTF curve, a vertical flipped reflection of the curve, that causes the valleys to become peaks. After that, the algorithm compares each individual TF-MTF curve with the preset input thresholds, deciding the classification (step 6) between Monofocal (MONO), Multifocal (MIOL) or Extended Depth of Focus (EDoF). This comparison considers only some of the peaks and valleys for the classification, and not all of them (as further discussed). Besides the classification, to each Periodic IOL configuration is attributed a score function (step 7) that, although it is an arbitrarily established merit function, it is based on physical characteristics that are desired for the IOL performance (further discussed in this section). Then, after these two pieces of information are obtained (the class and the score) for each individual configuration, the classification algorithm ends (step 8) and the results are exhibited in a 3D bar chart (section 4.1).

After the Peak Detection Function finds all of the TF-MTF peaks and valleys, two kinds of threshold are established: peak threshold (green colored line) and valley threshold (red colored line). They allow the algorithm to decide which regions of the TF-MTF curve are to be considered in the classification. The  $y$ -axis is the MTF normalized amplitude and the  $x$ -axis is the focus shift in millimeters.

The peak threshold specifies the minimum amplitude of the TF-MTF that still yields an acceptable contrast. If only one peak exceeds the peak threshold, the IOL is classified as monofocal. If there are two or more peaks with amplitude above the peak threshold, it can be classified as multifocal or EDoF. Therefore, it checks the valley threshold.

One limitation of the algorithm is that if the TF-MTF has only one peak, but that peak is large, which typically characterizes an EDoF IOL, it will classify the IOL as being Monofocal but with a large score value.

The valley threshold helps in differentiating the multifocal IOLs from the EDoF IOLs. If multiple peaks have an amplitude above the peak threshold, only the valleys that are between those peaks are considered for the classification between multifocal and EDoF IOLs. If all the valleys between two adjacent peaks fall below the valley threshold, the IOL configuration is classified as Multifocal. If at least one valley between two adjacent peaks does not fall below the valley threshold, the IOL is considered as having an Extended Depth of Focus.

The preset thresholds in this study are:

- Peak threshold: 0.2
- Valley threshold: 0.05 [11]

These are arbitrary values that were based on prior observation of the focal behavior of some simulated IOLs and have been chosen so that the peak threshold attempts to select which peaks are considered significant, while the valley threshold limits the width of a given peak, even setting boundaries to whether two adjacent bumps or hills are to be considered separate peaks or simply oscillations of a single peak. For instance, a monofocal aspheric IOL usually has a thin central peak, while an EDoF IOL often has a wider but lower peak. In contrast, a multifocal IOL can have multiple peaks with varying heights. A more thorough choice must be based on the standards to which the to be designed IOLs must comply.

The score function to calculate the performance of the TF-MTF of each IOL is the area under the curve. The trapezoidal integration technique was used, that consists of calculating the area below two adjacent TF-MTF points with a trapezoidal form and summing all the areas across the entirety of the curve [29]. Since the integration procedure registers the whole area under the curve, it cannot differentiate a curve with a single elevated central peak or a curve with smaller but multiple peaks: they both can generate a large area and receive a high ranking. Therefore, the strategy to use the area under the curve was to multiply it by the focus shift at 0 mm, to avoid this problem. It is important to notice that, although this strategy was arbitrarily chosen to confer a score that represents both a depth of focus increase and a high contrast related to the far focus, the equation can be easily adapted to account for different priorities or merit functions.

As such, none of the three possible IOL classes (monofocal, multifocal or EDoF) are privileged in any way.

Once the area under the TF-MTF curve is calculated, it is weighted by its respective MTF amplitude with a focus shift of zero millimeters, as indicated by Equation 6.

$$SCORE(i) = AREA(i) \times PEAK(i) \quad (6)$$

An important improvement point would be the insertion of optimization algorithms before the classification, to ensure that the simulated IOLs had the best in each of their respective categories, leading to optimal TF-MTF response curves. Also, this optimization algorithm could include not only the processing of the TF-MTF at a single spatial frequency, but at multiple frequencies. Other possible implementations would include different merit



functions that could be used simultaneously, such as the preclinical visual acuity and image simulation analysis. Although the latter options are discussed in sections 3.5 and 3.6 (and their results shown in sections 4.2 and 4.3), these merit functions were not included in any form of the optimization algorithm, nor they are used in the classification algorithm.

### **3.4 Units conversion**

Although being very similar in scope, the optical physics and the ophthalmic practice differ in some technical aspects, especially when it comes to optical interpretation of results. For instance, an optical engineer is more used to reporting depth of focus or depth of field in terms of distance, while in ophthalmology they are commonly expressed as additional power, in diopters. Both approaches are tackling the same topic, which is what happens to the image on the retina when an object moves closer or further from the eye.

Therefore, it is necessary to deploy a methodology to bridge the gap between these areas, by converting the units of one type into the other. It is also important to remember that there are some key differences between them. For example, the depth of focus does not depend on the eye geometry and refraction index. But additional refractive power depends on the effective focal length (*EFFL*) of the eye and also on the plane at which it is reported, such as the IOL plane, the corneal plane or the spectacles plane (the three most common).

This methodology is important because some important results are the preclinical defocus curves (as discussed earlier), that show the logMAR score versus the additional refractive power at the IOL plane for a given pupil aperture. The eye schematic used in the following deductions is shown in Figure 21.

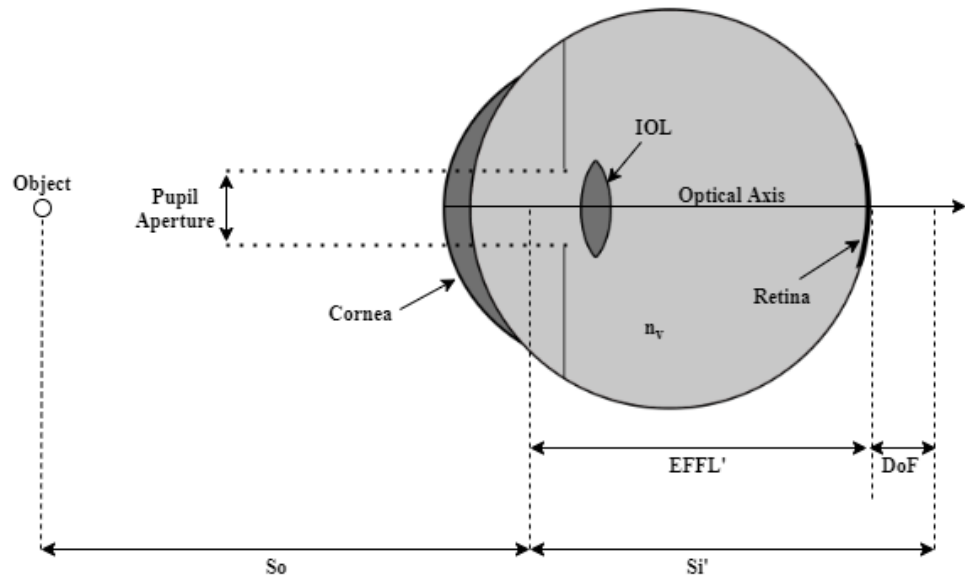


Figure 21 – Eye schematic used for unit conversion [author].

With Equation 7 , it is possible to calculate the image distance ( $S_i$ ) from the effective focal length ( $EFFL$ ), given in air, and the object distance ( $S_o$ ). Since the position where the image is formed is immersed in a medium different than air, the actual image position ( $S_i'$ ) must be scaled from the original image distance ( $S_i$ ) by Equation 8 ( $n_v$  is the refraction index of the vitreous humour). The same logic applies to the effective focal length (Equation 9).

$$\frac{1}{S_i} = \frac{1}{EFFL} - \frac{1}{S_o} \quad (7)$$

$$S_i' = n_v \cdot S_i \quad (8)$$

$$EFFL' = n_v \cdot EFFL \quad (9)$$

The depth of focus ( $DoF$ ) can be calculated (Eq. 10) by the difference between the actual image position ( $S_i'$ ) and the true effective focal length ( $EFFL'$ ).

$$DoF = (S_i' - EFFL') \quad (10)$$

The problem is, that the simulation software only exhibits  $EFFL$  and not  $EFFL'$ . Therefore, the conversion is done by substituting Eqs. 8 and 9 in Eq. 10, to provide an equation that is scaled to the material medium (Eq. 11).

$$DoF = n_v(S_i - EFFL) \quad (11)$$

With the previous equation it would not be possible to calculate the depth of focus, since the image distance is usually located in a position beyond the retina plane. Therefore, it is necessary to rewrite the previous equation (Eq. 11) as a function of the object distance and the effective focal length (using Eqs. 6). The deduction process is shown in Equations 12 and 13.

$$DoF = n_v \left( \frac{1}{\frac{1}{S_i}} - EFFL \right) \quad (12)$$

$$DoF = n_v \left( \frac{1}{\frac{1}{EFFL} - \frac{1}{S_o}} - EFFL \right) \quad (13)$$

The following equation (Eq. 14) converts the Depth of Focus (**DoF**) to additional refractive power on the IOL plane (**D<sub>IOL</sub>**; in diopters).

$$D_{IOL} = \frac{1}{EFFL} - \frac{1}{(EFFL + DoF)} \quad (14)$$

With all these considerations, it is possible to represent the units conversion through the following graphs (Figure 22 and Figure 23):

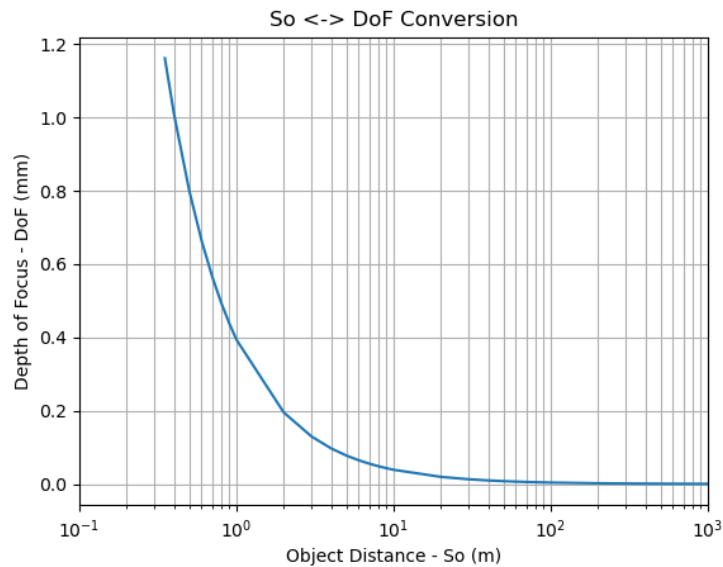


Figure 22 – Conversion of object distance ( $S_o$ ) to depth of focus ( $DoF$ ) [author].

In Figure 22, when the object comes closer to the eye and is still kept in focus (represented by a decrease on the  $x$ -axis) represents an increase in the depth of focus (DoF). This is in accordance to the phenomena shown in Figure 16 (section 2.5), where an approaching object displaces the TF-MTF curve to a plane behind the retinal plane causing the focus to shift a few millimeters. With Equation 13, it is possible to notice that this translation between the distance shifted by the object and the focus shift on the retinal plane happens in a hyperbolic fashion.

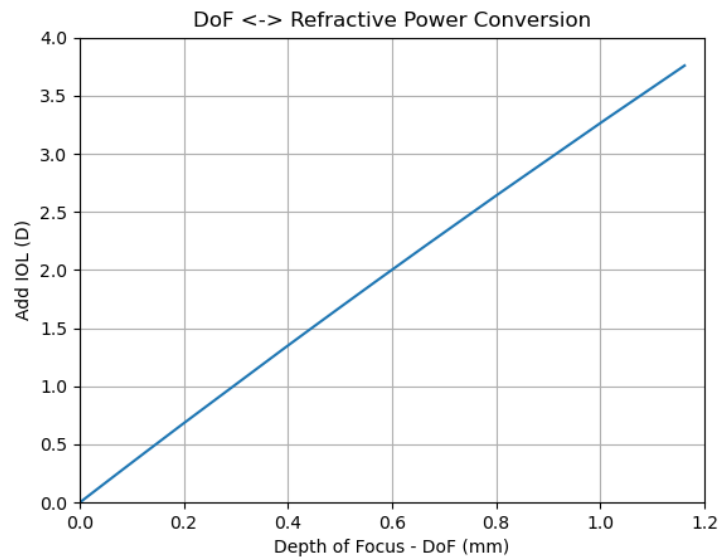


Figure 23 – Conversion of depth of focus to refractive power at the IOL plane [author].

The graph shown in Figure 23 is an implementation of Equation 14, where not only it is possible to associate the depth of focus with an approaching object (previously explained), but with an additional refractive power in diopters at the intraocular lens plane (Add IOL). It is possible to notice that this conversion happens in a linear manner.

It is convenient to use this conversion because the TF-MTF exhibits the contrast curve as a function of the focus shift (in millimeters). But in clinical practice and lens prescriptions the additional refractive power is often used and referenced, for instance, on the IOL plane.

### 3.5 Image size calculations

The Snellen eye chart is commonly used in clinical practice to evaluate the visual acuity of patients [30]. It is based on Figure 24 and Equation 15:

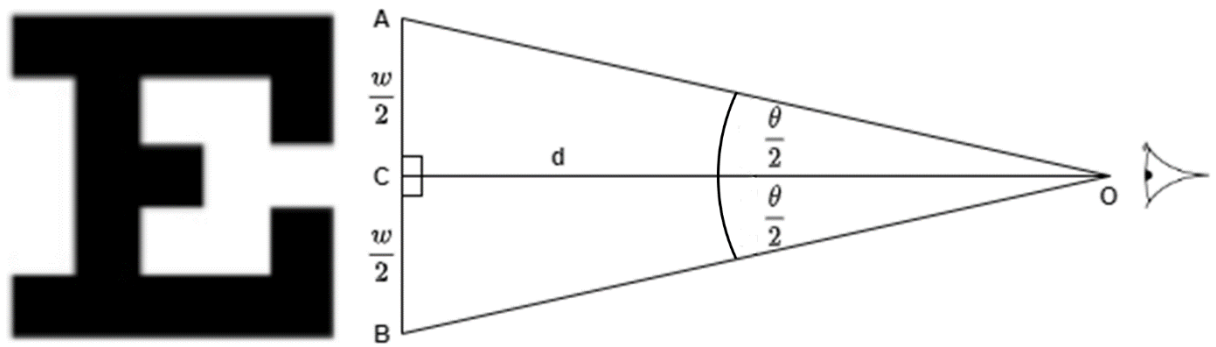


Figure 24 – Visual angle representation [author].

$$\theta = 2 \tan^{-1} \left( \frac{w}{2d} \right) \quad (15)$$

Where  $w$  is the object height,  $d$  is the distance from the eye and  $\theta$  is the visual angle.

It is important to reinforce that each visual acuity represented on the Snellen chart is associated with a pre-established letter size that is related to a fixed visual angle for a distance of 20 feet. For instance, if the letter in Figure 24 represents a visual acuity of 20/40 on the Snellen chart (line 5 of Figure 17 in section 2.6), it is associated with a visual angle of 10 minutes of arc for an object located 20 feet ( $\sim 6$  m) away from the eye. Substituting these values on Equation 15, it is possible to estimate an object height  $w = 17.45$  mm.

Once the object heights are calculated for a myriad of visual acuities, it is possible to estimate the image size that is formed on the retinal plane. Surely, this conversion depends on the geometrical and material characteristics of the optical system under test, which is expressed by the Effective Focal Length (*EFFL*). Since the optical system under test has an *EFFL* of 17.0118 mm (using the spherical IOL as the base lens) the height of the image formed on the image plane can be calculated by means of Equation 16.

$$\Delta_i = \frac{\Delta_o}{\left( \frac{d}{EFFL} \right) - 1} \quad (16)$$

Where  $\Delta_i$  is the image height,  $\Delta_o$  is the object height ( $w$ ) and  $d$  is the distance from the object to the eye. For a visual acuity of 20/40, an object height ( $w$ ) of 17.45 mm and an optical system with an *EFFL* equal to 17.0118 mm, the correspondent image size  $\Delta_i$  is 49.62  $\mu\text{m}$ .

Each visual acuity indicated by a Snellen index (20/10, 20/20, and so on) is based on a different visual angle. At the same distance of 6 m (roughly 20 ft), bigger letters correspond to

increased visual angles. Therefore, an arbitrary set of Snellen indices are expressed in Table 3 with their respective visual angles, their associated object heights (Equation 15) and image heights (Equation 16).

*Table 3 – Image height calculations for an EFFL = 17.0118 mm [author].*

Snellen	Visual angle (arc min)	Object height (mm) @ 6 m	Image Height ( $\mu\text{m}$ )
20/10	2.5	4.36	12.41
20/20	5	8.73	24.81
20/32	8	13.96	39.70
20/40	10	17.45	49.62
20/100	25	43.63	124.07

### 3.6 Preclinical visual acuity

According to [31] it is possible to estimate the correlation between the MTF and a preclinical visual acuity score in logMAR, generating a defocus curve as widely used in the ophthalmic community.

It is done by computing the area below the MTF curve ( $MTF_a$ ) until a frequency of 50 lp/mm. Since the MTF amplitude varies between 0 and 1, the maximum area achievable by the MTF function is constrained inside the rectangle with an area of 50. Therefore, each individual MTF area is normalized by this value and the visual acuity (V.A.) in a logMAR score is computed using Equation 17.

$$V.A. (MTF_a) = \frac{0.085}{MTF_a} - 0.21 \quad (17)$$

Where the coefficients (0.085 and -0.21) are obtained through visual inspection of [30]. The general behavior for the equation can be seen in Figure 25.

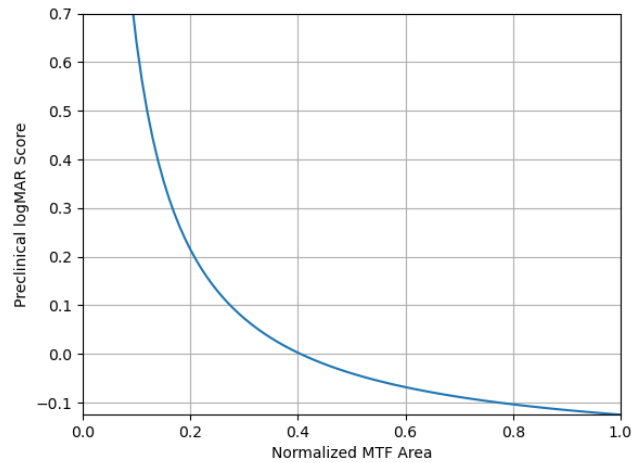


Figure 25 – Conversion of normalized MTF area to preclinical logMAR score [author].

The first noticeable behavior is that when the normalized area under the MTF curve increases, the preclinical logMAR score decreases. This is in accordance to the general logMAR behavior, since more negative values represent a better visual acuity and vice versa. The correlation between different visual acuities and the logMAR score can be seen in

Table 4.

Table 4 – Correlation between visual acuity (Snellen) and logMAR score [author].

Visual Acuity (Snellen)	logMAR Score
20/10	-0.3
20/15	-0.125
20/16	-0.1
20/20	0
20/25	0.1
20/32	0.2
20/40	0.3

Using the Equation 17, it is possible to notice that when the area under the normalized MTF curve is maximized (theoretically equals to 1), the preclinical logMAR score has a value of -0.125. This is the maximum logMAR score that can be predicted with this equation.

## 4 RESULTS AND DISCUSSION

In this section it is presented the main result through a bar chart that simultaneously exhibits the classification and the score given to each simulated IOL. Some of the simulated IOLs are selected, being one monofocal, one multifocal and all EDoF IOLs. After the selection, the preclinical visual acuity charts are shown and analyzed. They are followed by the image simulation of a 20/32 letter located at four different distances from the eye.

It is important to note that although the preclinical visual acuity and the image simulations are both shown in this section, they are not considered in the classification algorithm. The algorithm as developed so far only takes into account the Through-Focus MTF response.

The results were obtained for a wavelength of 550 nm light (green color), an effective lens position of 0.102 mm (position inside the 3 mm capsular bag), and a 3 mm pupil aperture. The effective focal length is 17.0118 mm.

### 4.1 3D bar chart

The generated three-dimensional bar chart is the main resulting contribution of this study (Figure 26). It exhibits all of the considered sinusoidal amplitudes and frequencies for the Periodic surface and aids the lens designer in the identification of the most suitable parameters to yield a given class of lenses. It is important to reaffirm that the main goal is to find configurations that can lead to lenses with an Extended Depth of Focus. The bar height represents the Score and the color represents the IOL class. Five IOLs were chosen for the purposes of comparison: the monofocal (MONO) and multifocal (MIOL) were arbitrarily chosen close to each other and among those with a high score ( $z$  axis), reasonable and equal sinusoidal amplitude between them, and featuring also close sinusoidal-pattern frequencies; the only three EDoF samples, according to the classification algorithm, have also been selected.

It is important to comment that the colors of each bar in the 3D graph represent the classification results *per se*, while each respective height represents an assigned score through a customized heuristic. This heuristic considers both the area under the Through-Focus MTF curve and the height of the central peak, both at 50 lp/mm (as previously discussed in section 3.3).



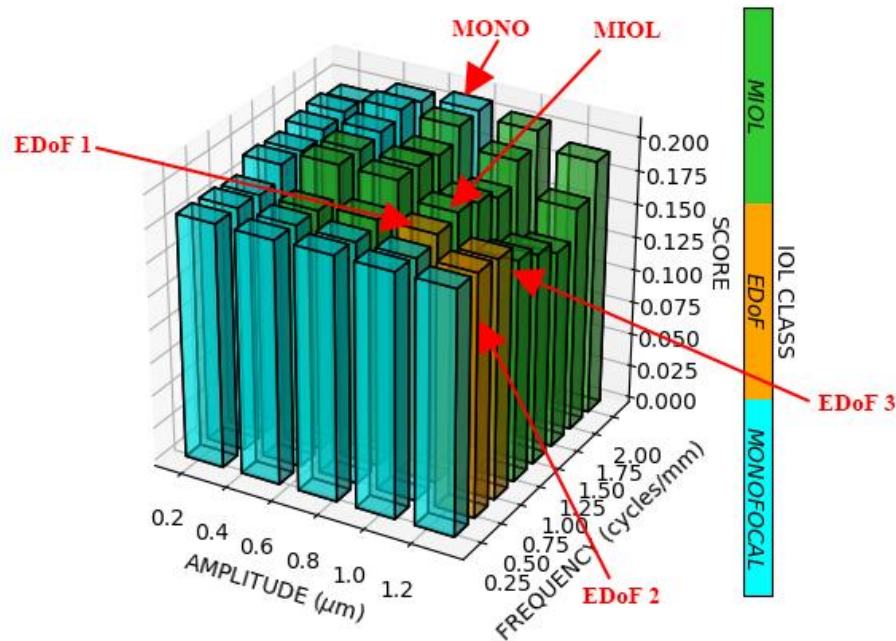


Figure 26 – IOL score and classification as a function of the designed sinusoidal amplitudes and frequencies [author].

The classification summary is show in Table 5.

Table 5 – Classification summary [author].

	Monofocal	Multifocal	EDoF
IOL class/Total number of IOLs	19/40	18/40	3/40

The selected IOLs are shown in Table 6.

Table 6 – Periodic parameters of the selected IOLs [author].

IOL	Amplitude (mm)	Frequency (peaks/mm)
EDoF 1	1.00	0.75
EDoF 2	1.25	0.50
EDoF 3	1.25	0.75
Monofocal	0.75	2.00
Multifocal	1.00	1.00

This algorithm highly relies on a good selection of the peak and valley thresholds. For instance, if the peak threshold is too high, many IOLs are classified as Monofocal, because most of the secondary peaks will not reach the threshold. If it is low, the procedure tends to classify most IOLs between EDoFs or MIOLs.

If the valley threshold is high, most valleys will fall below it, therefore the algorithm will consider the neighboring peaks to be apart enough from one another. Then, it will classify the IOL as Multifocal (MIOL). If the valley threshold is too low, many IOLs will be classified as EDoFs, since neighboring peaks are considered as being extensions of the the main central peak.

The three EDoF IOLs found during the classification methodology have the characteristics shown in Table 7.

Table 7 – Extended depth of focus IOLs TF-MTF characteristics at 50 lp/mm [author].

	Amplitude (central peak)	Amplitude (secondary peak)
EDoF 1	0.68	0.31
EDoF 2	0.77	0.22
EDoF 3	0.64	0.34

Note that the compared amplitudes are the central peak and the secondary peak, that appears between -0.2 mm and -0.4 mm of focus shift for any of the EDoF IOLs. This value corresponds to the general region where the secondary peaks occur across the selected IOLs. It corresponds to an object located roughly at 0.66 m from the eye. The corresponding TF-MTF curves for all of the 5 IOLs are shown in Figure 27 through Figure 31.

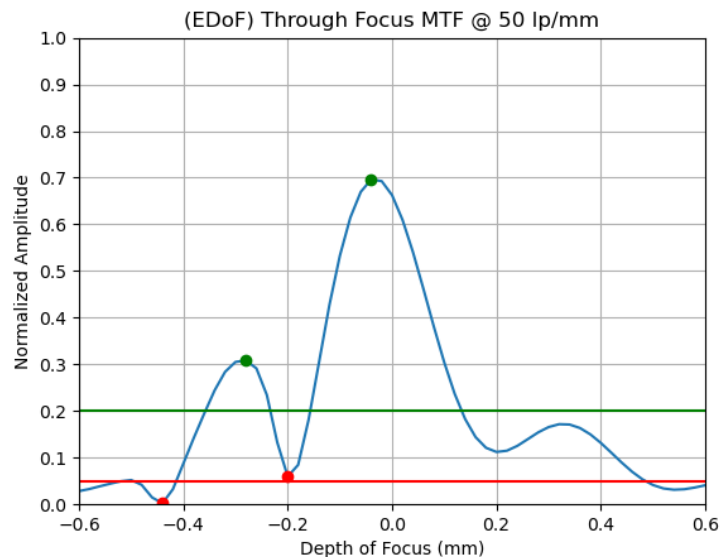


Figure 27 – Through-Focus MTF curve for EDoF 1 [author].

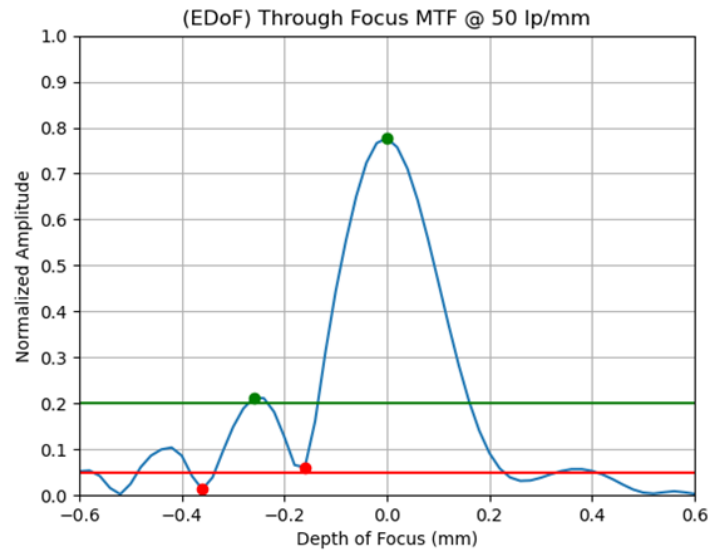


Figure 28 – Through-Focus MTF curve for EDoF 2 [author].

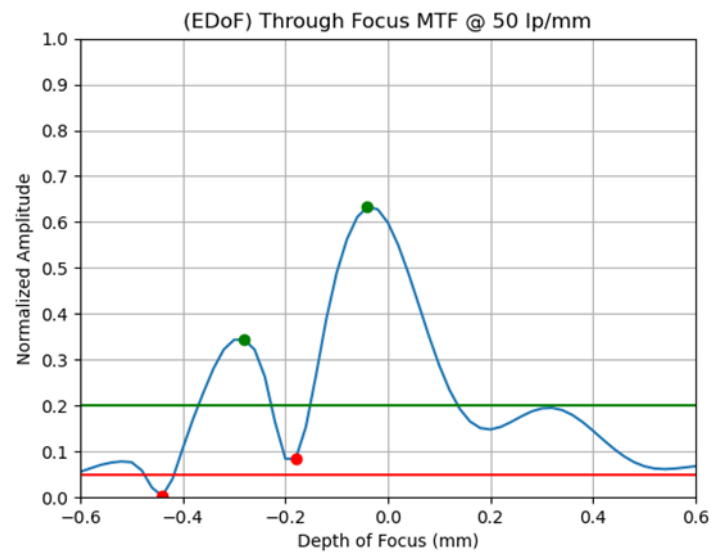


Figure 29 – Through-Focus MTF curve for EDoF 3 [author].

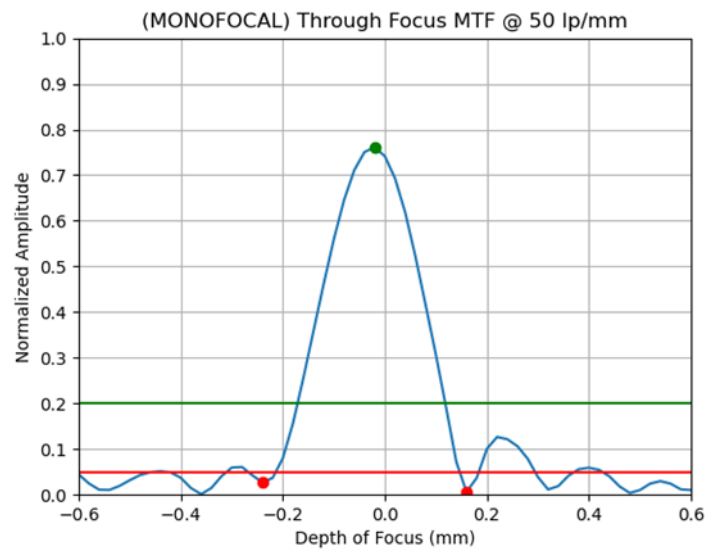


Figure 30 – Through-Focus MTF curve for Monofocal IOL [author].

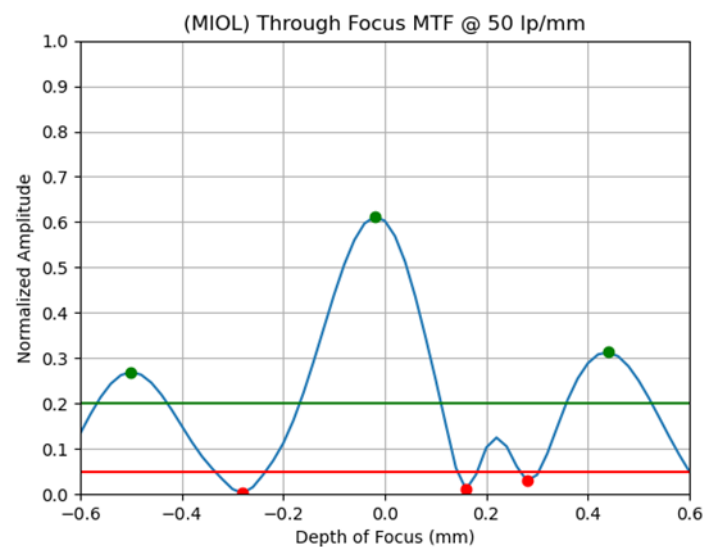


Figure 31 – Through-Focus MTF curve for Multifocal IOL [author].

It is possible to notice that for each of the EDoF Through-Focus MTF curves, the valleys between the two peaks (red dots) do not fall below the valley threshold value (red lines). Therefore, the algorithm considers that the secondary peak provides an extended range of focus (and not a secondary focus), classifying the IOLs as EDoF instead of multifocal.

According to [32], the values of contrast exhibited in Table 7 are well within the range of the TF-MTFs of commercial EDoF IOLs, such as the TECNIS Symphony ZXR00 (Johnson&Johnson) and the AT LARA 829MP (Carl Zeiss Meditec). The Through-Focus MTF response at 50 lp/mm is shown in Figure 32.

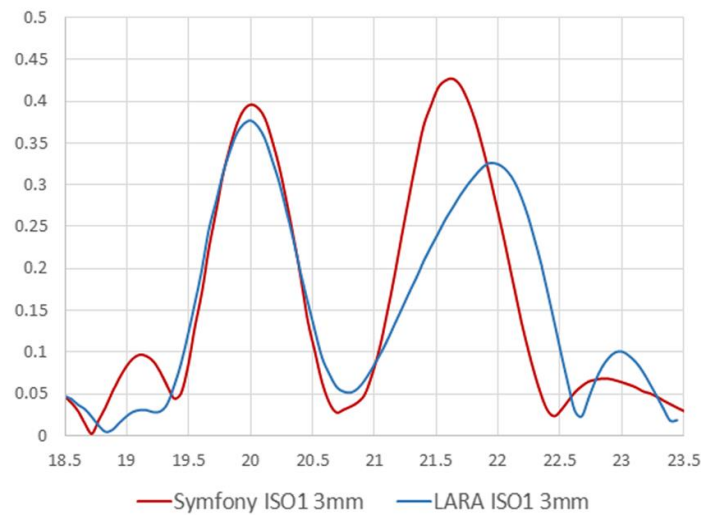


Figure 32 – Comparison between Symphony and AT LARA IOLs [32].

It is important to indicate that the ISO eye model was used for the IOL comparison. Also, the  $x$ -axis scale is measured in diopters and not focus shift in millimeters. The mathematical parameters of both IOLs is not known, therefore it is impossible to estimate the Effective Focal Length (*EFFL*) and, consequently, the accurate conversion from diopters to focus shift. What is known is that both IOLs were designed with 20 D of additional refractive power and a secondary focus around +1.5 or +2 D. If only the refractive powers are compared, it is possible to notice that both the main central peak amplitude (@ 20 D) and the secondary peak amplitude (@ ~22 D) are around 0.4, which is well within the Periodic IOL Through-Focus response range.

## 4.2 Visual acuity

Using [31] as previously discussed in section 3.6 the visual acuity graphs were generated. They were simulated with optical apertures (pupil sizes) of 3.0, 4.5 and 6.0 mm of diameter. The selected EDoF IOL was the “EDoF 1”. The IOL was arbitrarily chosen between the three EDoF IOLs found so the following graphs would not be crowded with information. The same IOL was selected for the purpose of image simulation on section 4.3. The results can be seen in Figure 33 to Figure 35.

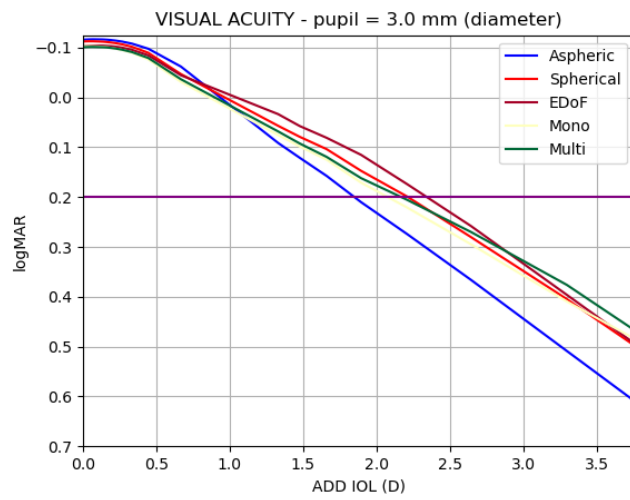


Figure 33 – logMAR plot for pupil diameter of 3.0 mm [author].

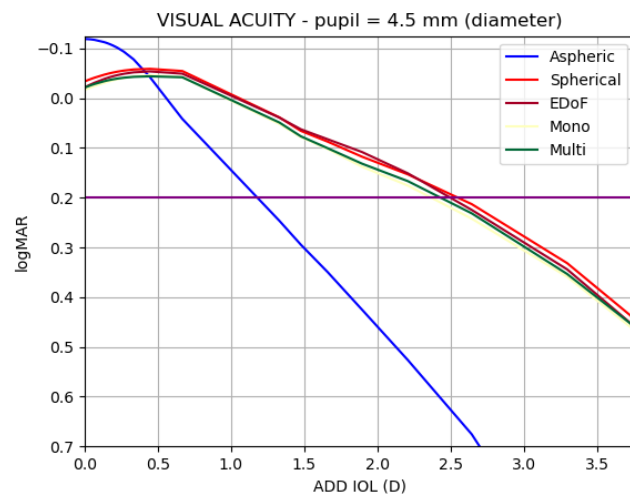


Figure 34 – logMAR plot for pupil diameter of 4.5 mm [author].

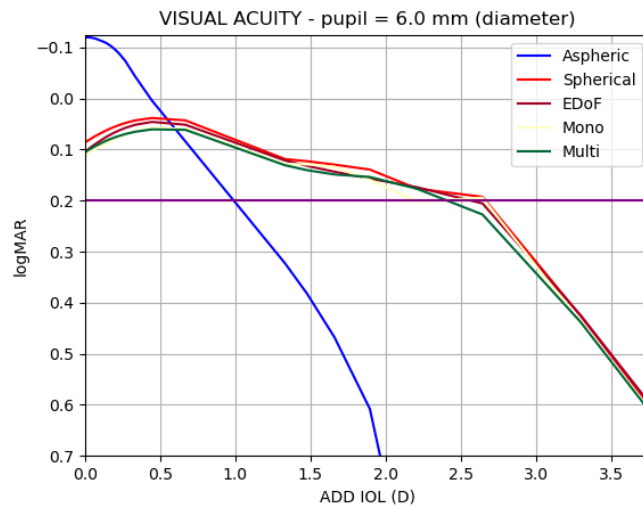


Figure 35 – logMAR plot for pupil diameter of 6.0 mm [author].

It is possible to notice that independently from the pupil aperture, the logMAR score at 0 D for the aspheric is the higher of the set as expected, since it has the best contrast for the distant focus. All of the other IOLs follow the tendency of the spherical logMAR. The monofocal IOL although exhibits a performance better than the aspheric, it is not enough to be classified as EDoF according to [10], since the dioptric difference at logMAR 0.2 is lower than 0.5 D. Also, note that the multifocal IOL monotonically decreases the logMAR score after 0.5 D, which can be explained because all of the simulated IOLs follow the general behavior of the spherical IOL. When the pupil aperture increases, if the curves cross logMAR 0.2 at a higher refractive power, it means that the object moves closer to the eye and its image still preserves have an acceptable contrast. It is desired that for a 3 mm pupil aperture, this crossing point happens with a refractive power as high as possible, which means a given 20/32 letter could be seen at a distance closer to the eye. There was an expectation that the aspheric lens would have a higher crossing point at logMAR 0.2 for a 3 mm aperture when compared with other apertures. This happens because the aspheric IOL rapidly decreases performance as the pupil increases in size.

Since the EDoF classification requirements [10] are for a 3.0 mm pupil diameter, we must pay special attention to (Figure 33). It is possible to notice that only the EDoF IOL meets the first two criteria. The EDoF line crosses 0.2 logMAR at roughly 2.3 D, while the best aspheric IOL has about 1.75 D. According to the support graphs in Chapter 3, an object at 66 cm from the eye has about 2.0 D of additional refractive power at the IOL plane. This can also be verified since the EDoF curve is always above the purple line up about 2.3 D. Unfortunately,

the last criterion is not met, since at 0 D the logMAR score difference to the aspheric IOL should be no larger than 0.1. Note that the EDoF IOL has about 0.1 logMAR score in that situation.

On the other hand, Figure 34 and Figure 35 show that the EDoF lens has a great depth of focus when the pupil size increases. This happens mainly due to the base lens being designed as being spherical. Therefore, the sinusoidal configurations were expected to show little deviation from the base spherical IOL.

### 4.3 Image simulation

The results shown in Table 8 through Table 11 are the visual representations of a given letter at the specified object distances for each of the 5 IOLs: aspheric (ASP), spherical (SPH), monofocal (MONO), multifocal (MIOL) and extended depth of focus (EDoF 1). The image simulations were done for three different pupil diameters (3.0, 4.5 and 6.0 mm), and each result comprises the image projected on the retina for the object (letter E) with fading contrast levels with the following values: 100%, 77%, 55%, 33% and 11%. The intent is to represent situations of low luminosity, for instance, driving at night, where the object contrast is reduced.

Since the following tables are a representation of a 20/32 Snellen visual acuity, the analysis proceeds at the intersection between the purple lines in Figure 33 through Figure 35 and the logMAR curve for each IOL and each pupil size. Therefore, it is possible to notice that for any given pupil, the aspheric IOL crosses logMAR 0.2 at a lower power than the other IOLs.

It is also relevant to mention the choice of the object distances. Usually, each patient has different requirements on activities that require objects placed at different distances and different lighting conditions (which reflects on the pupil size). When an object is placed at 1 km from the eye, for instance, one patient might have night driving habits, which happen in low luminosity scenarios. This means that the pupil often exhibits a larger diameter than when the patient tries to see a distant building in broad daylight. On the other hand, as the object comes closer to the eye, e.g. 2 m, it usually represents the distance that a person usually watches television, for example. In this scenario, usually the luminosity conditions are intermediary, with the room dimly lit. The object located at 0.66 m from the eye represents a situation such as reading on a computer screen, doing domestic chores or talking with another person. In these scenarios, usually the object is well illuminated (such as an illuminated desk) or is self-lit (such as a screen).

Therefore, four different distances were chosen to be representative of different activities, but also the chosen pupils were chosen to represent different levels of luminosity.



The 3.0-mm pupil represents a high luminosity condition, called photopic. The 4.5-mm pupil was chosen to represent an intermediate scenario, called mesopic. And the 6.0-mm pupil represents a low luminosity situation, such as driving at night, called scotopic.

It is also important to remember that, associated with each of the four selected distances, there is an associated image height projected on the image plane, for any desired Snellen visual acuity (in this case, 20/32). This calculation is extremely important and was previously discussed in section 3.5. Therefore, the image height used was of 39.70  $\mu\text{m}$ , associated with an object placed 6 m away from the eye for an *EFFL* of 17.0118 mm. It is important to notice that in this simulation the image height value does not change as the object approaches the eye, with the intent of maintaining the same visual angle across all of the selected distances.

Table 8 – Visual acuity of a 20/32 letter at 1 km from the eye [author].

20/32	Pupil 3.0 mm					Pupil 4.5 mm					Pupil 6.0 mm				
ASP	<b>E</b>	<b>E</b>	<b>E</b>	<b>E</b>	<b>E</b>	<b>E</b>	<b>E</b>	<b>E</b>	<b>E</b>	<b>E</b>	<b>E</b>	<b>E</b>	<b>E</b>	<b>E</b>	<b>E</b>
SPH	<b>E</b>	<b>E</b>	<b>E</b>	<b>E</b>	<b>E</b>	<b>E</b>	<b>E</b>	<b>E</b>	<b>E</b>	<b>E</b>	<b>E</b>	<b>E</b>	<b>E</b>	<b>E</b>	<b>E</b>
MONO	<b>E</b>	<b>E</b>	<b>E</b>	<b>E</b>	<b>E</b>	<b>E</b>	<b>E</b>	<b>E</b>	<b>E</b>	<b>E</b>	<b>E</b>	<b>E</b>	<b>E</b>	<b>E</b>	<b>E</b>
MIOL	<b>E</b>	<b>E</b>	<b>E</b>	<b>E</b>	<b>E</b>	<b>E</b>	<b>E</b>	<b>E</b>	<b>E</b>	<b>E</b>	<b>E</b>	<b>E</b>	<b>E</b>	<b>E</b>	<b>E</b>
EDoF 1	<b>E</b>	<b>E</b>	<b>E</b>	<b>E</b>	<b>E</b>	<b>E</b>	<b>E</b>	<b>E</b>	<b>E</b>	<b>E</b>	<b>E</b>	<b>E</b>	<b>E</b>	<b>E</b>	<b>E</b>

From Table 8 it is possible to notice that for objects at 1 km from the eye, the aspheric IOL presents the best performance as expected. All of the other IOLs present similar contrast for smaller apertures but exhibit a blur around the letter as the aperture increases. In this situation, one would usually prefer an aspheric IOL, not only because it exhibits a better contrast when compared with the other IOLs but because the contrast practically does not change across different pupil sizes.

Table 9 – Visual Acuity of a 20/32 letter at 6 m from the eye [author].

20/32	Pupil 3.0 mm	Pupil 4.5 mm	Pupil 6.0 mm
ASP			
SPH			
MONO			
MIOL			
EDoF 1			

As the object gets closer to the eye Table 9, the aspheric IOL performance decreases while the others remain roughly the same. It is possible to notice the aperture effect when observing the aspheric IOL for different apertures, as it blurs more evidently. Here the advantages of the other IOLs begin to show, where the simulated letter can still be seen accurately, even when the blur is present. This object distance of 6 m (roughly 20 ft.) was used because it represents the distance at which the test using the Snellen eye chart is usually performed in clinical practice.

Table 10 – Visual Acuity of a 20/32 letter at 2 m from the eye [author].

20/32	Pupil 3.0 mm	Pupil 4.5 mm	Pupil 6.0 mm
ASP			
SPH			
MONO			
MIOL			
EDoF 1			

When the object is at a 2 m distance (Table 10), the aspheric IOL performance greatly deteriorates, as expected, since it provides the worst depth of focus of the set. The other IOLs, although also blurred, can be easily distinguished for greater apertures (which does not happen with the aspheric IOL). At this object distance, it is not possible to distinguish the simulated

letter for the aspheric IOL even for intermediate pupils, which gives more credit to the other simulated IOLs. With the three previous results (Tables 8, 9 and 10), it is possible to perceive that the simulated IOLs have a reasonable photopic contrast (associated with the smaller optical aperture of 3.0 mm).

*Table 11 – Visual Acuity of a 20/32 letter at 0.66 m from the eye [author].*

20/32	Pupil 3.0 mm	Pupil 4.5 mm	Pupil 6.0 mm
ASP			
SPH			
MONO			
MIOL			
EDoF 1			

If the object is located at a distance even closer to the eye (Table 11), it becomes very hard to observe any of the 20/32 letters. Only when the pupil aperture is at 6 mm it is possible to note a subtle contour. Even in this case, it is verified that the aspheric has the worst performance of the set. One interesting effect is that the sharpness seems to increase with bigger apertures, although often this situation where the object is this close, it is usually well illuminated (smaller apertures).

It is possible to notice that when the object is placed at 0.66 m from the eye, the contrast increases for a 6.0 mm pupil. This phenomena can be explained by the gradual insertion of the sinusoidal peaks as the optical aperture increases, forcing part of the refracted rays to converge around the focal point. Therefore it is possible to see on the right column (Table 11) the contour of the simulated letter, which is not possible for smaller apertures.

As previously discussed, the Periodic IOLs have been modelled using the spherical IOL as the base lens, which means their logMAR scores tend to follow the spherical behavior, for any given set of Periodic parameters.

## 5 CONCLUSIONS

Through this study it was possible to investigate the different types of IOLs present on the market, as well as the procedure on how to design a lens using the geometric and material characteristics for any given refractive power. It also presented an insight on features of different eye models. It was possible to learn about the raytracing process and also about useful merit functions to allow the comparison of the optical performance of distinct IOLs.

The study also enabled the understanding of the variables commonly used in optics and their correspondent in ophthalmic practice, which helped bridge the gap between these two fields. An algorithm was proposed to help the classification of different periodic IOL configurations among different types of optical performances. The algorithm was capable of sorting the lens performance as monofocal, multifocal or extended depth of focus. This classification occurs by comparing the peaks and valleys of an important optical merit function, which is the Through-Focus MTF.

The different periodic IOL configurations led to a variety of optical performance, including 3 IOLs classified as having an extended depth of focus (EDoF). These lenses were investigated and compared with two EDoF IOLs already present on the market, having analog values of contrast across different TF-MTF regions (for the same spatial frequency of 50 lp/mm). The simulated IOLs exhibited logMAR score of 0.2 up to an object distance of roughly 0.6 m, for a 3.0-mm pupil size. Although one EDoF requirements was not satisfied, e.g. the logMAR score difference at 0 D to the monofocal aspheric IOL was greater than 0.1, the other requirements were met. Meanwhile, the selected EDoF IOLs secondary foci were mainly located between a focus shift of -0.2 and -0.4 mm, which is equivalent to an object distance from 2 m to 1 m, respectively. In contrast, the multifocals IOL exhibited secondary foci of at least -0.4 mm of focus shift, which is equivalent to objects located at a maximum distance of 1 m. Therefore, there is a noticeable difference between the nearest field shown through the TF-MTF analysis and the preclinical visual acuity curve. This could be explained as the TF-MTF only considers one specific spatial frequency at a time, while the preclinical visual acuity considers all frequencies from 0 to 50 lp/mm,

One interesting fact is that even though the TF-MTF curve for the periodic IOL classified as multifocal present secondary peaks that are separated from the primary peak, the preclinical visual acuity curve showed a monotonical decrease in contrast, in a similar manner to EDoF IOLs. This means that only classifying an intraocular lens based on the TF-MTF curve

(at a single spatial frequency) is insufficient to determine if it behaves as multifocal or EDoF. The visual acuity must also be taken into account.

After classifying the various simulated topologies, they were compared with some well-established off-the-shelf IOLs. Some of the interesting IOL topologies from different classes were chosen and a visual acuity analysis was made, which was represented by the preclinical defocus curve and image simulations. The preclinical defocus curve gives an excellent method to evaluate the overall IOL performance, since it is based on the MTF curve for many spatial frequencies and not one specifically, in contrast to the Through-Focus MTF curve.

The image simulations were configured by adjusting the image size according to Snellen patterns for a given 20/32 letter (letter E), which corresponds to a logMAR score of 0.2. This score is important because it is related to the ANSI-standard requirements for an IOL to be classified as having an extended depth of focus. The simulated letter was then placed at varying distances from the eye, to evaluate the effect of the resulting depth of focus.

This study was important to promote expertise in lens design for the ophthalmic optics field and to investigate the specifics of intraocular lens performance analysis. It was possible to understand the parametric influences on different merit functions, enabling a systematic analysis of optical performance, as practiced in the ophthalmic scenario for intraocular lenses.

## REFERENCES

- [1] STRENK, Susan A.; STRENK, Lawrence M.; KORETZ, Jane F. The mechanism of presbyopia. *Progress in retinal and eye research*, v. 24, n. 3, p. 379-393, 2005.
- [2] KOHNEN, Thomas. Nondiffractive wavefront-shaping extended range-of-vision intraocular lens. **Journal of Cataract & Refractive Surgery**, v. 46, n. 9, p. 1312-1313, 2020.
- [3] DE LUIS EGUILEOR, B. et al. Differences in intermediate vision: Monofocal intraocular lenses vs. monofocal extended depth of focus intraocular lenses. **Archivos de la Sociedad Española de Oftalmología (English Edition)**, v. 95, n. 11, p. 523-527, 2020.
- [4] HONG, X.. **Intraocular lens with extended depth of focus**. Alcon Laboratories. Patent US 2010/0161051A1, deposited on December 9<sup>th</sup>, 2009.
- [5] LOGOTHETIS, N. K. Visual competition. *Nature Reviews Neuroscience*, v. 3, n. 1, p. 13-23, 2002.
- [6] GUTMAN, A. S.; SHCHESYUK, I. V.; KOROLKOV, V. P. Optical testing of bifocal diffractive-refractive intraocular lenses using Shack-Hartmann wavefront sensor. In: *Optical Micro-and Nanometrology III*. International Society for Optics and Photonics, 2010. p. 77181P.
- [7] Saleh, B. E., & Teich, M. C. (2019). *Fundamentals of photonics*. John Wiley & sons.
- [8] [https://en.wikipedia.org/wiki/File:Conic\\_Sections.svg](https://en.wikipedia.org/wiki/File:Conic_Sections.svg) (accessed on November 30<sup>th</sup>, 2020, at 10:36 PM)
- [9] <https://en.wikipedia.org/wiki/Spheroid#/media/File:Spheroids.svg> (accessed on November 30<sup>th</sup>, 2020, at 10:36 PM)
- [10] ANSI Z80.35-2018. American Vision Standards Institute, Inc., The Vision Council, The Accredited Committee Z80 for Ophthalmic Standards, 2019.
- [11] [https://www.accessdata.fda.gov/cdrh\\_docs/pdf/P930014S126C.pdf](https://www.accessdata.fda.gov/cdrh_docs/pdf/P930014S126C.pdf) (accessed on November 30<sup>th</sup>, 2020, at 10:36 PM)

- [12] ALMEIDA, Marina Storani de; CARVALHO, Luis Alberto. Different schematic eyes and their accuracy to the in vivo eye: a quantitative comparison study. *Brazilian Journal of Physics*, v. 37, n. 2A, p. 378-387, 2007.
- [13] NORRBY, Sverker et al. Model eyes for evaluation of intraocular lenses. *Applied optics*, v. 46, n. 26, p. 6595-6605, 2007.
- [14] ATCHISON, David A. Optical models for human myopic eyes. *Vision research*, v. 46, n. 14, p. 2236-2250, 2006.
- [15] LI, Shi-Ming et al. Paraxial schematic eye models for 7-and 14-year-old Chinese children. *Investigative Ophthalmology & Visual Science*, v. 56, n. 6, p. 3577-3583, 2015.
- [16] BREZNA, Wolfgang; DRAGOSTINOFF, Nikolaus; PRINZ, Martin. Human eye modeling for intraocular lens design and for calculating intraocular lens power. *IFAC Proceedings Volumes*, v. 45, n. 18, p. 534-539, 2012.
- [17] Liou, H. L., & Brennan, N. A. (1997). Anatomically accurate, finite model eye for optical modeling. *JOSA A*, 14(8), 1684-1695.
- [18] Zemax, L. L. C. (2013). *OpticStudio User Manual*. Zemax LLC.: Kirkland, WA, USA.
- [19] <https://courses.lumenlearning.com/boundless-physics/chapter/lenses/#:~:text=The%20thin%20lens%20equation%20quickly,hi%2Fh>o). (accessed on November 30<sup>th</sup>, 2020, at 10:36 PM)
- [20] Hecht, E. (2012). *Optics*. Pearson Education India.
- [21] WATSON, Andrew B.; YELLOTT, John I. A unified formula for light-adapted pupil size. *Journal of vision*, v. 12, n. 10, p. 12-12, 2012.
- [22] Artal, P. (Ed.). (2017). *Handbook of Visual Optics, Two-Volume Set*. CRC Press.
- [23] BAKARAJU, Ravi C. et al. Finite schematic eye models and their accuracy to in-vivo data. *Vision research*, v. 48, n. 16, p. 1681-1694, 2008.

- [24] KAISER, Peter K. Prospective evaluation of visual acuity assessment: a comparison of snellen versus ETDRS charts in clinical practice (An AOS Thesis). Transactions of the American Ophthalmological Society, v. 107, p. 311, 2009.
- [25] [https://en.wikipedia.org/wiki/Snellen\\_chart#/media/File:Snellen\\_chart.svg](https://en.wikipedia.org/wiki/Snellen_chart#/media/File:Snellen_chart.svg) (accessed on November 30<sup>th</sup>, 2020, at 10:36 PM)
- [26] COSTA, D., MONTEIRO, D.W.d.L., *Methodology for the Classification of an Intraocular Lens with an Orthogonal Bidimensional Refractive Sinusoidal Profile*. Congresso Brasileiro de Engenharia Biomédica (CBEB), 2020.
- [27] COSTA, D., MONTEIRO, D.W.d.L., *Methodology for the Classification of an Intraocular Lens with an Orthogonal Bidimensional Refractive Sinusoidal Profile*. SPIE Photonics East, 2020.
- [28] No, I. S. 11979-2 (2014) Ophthalmic Implants-Intraocular Lenses-Part 2: optical properties and test methods. *International Organization for Standardization, Geneva, Switzerland*.
- [29] Atkinson, Kendall E. (1989), *An Introduction to Numerical Analysis* (2nd ed.), *New York: John Wiley & Sons*, ISBN 978-0-471-50023-0
- [30] Howett, Gerald L. "Size of Letters Required for Visibility as a Function of Viewing Distance and Observer Visual Acuity". *U.S. Government Publishing Office*. United States Department of Commerce. National Bureau of Standards.
- [31] Alarcon, Aixa, et al. "Preclinical metrics to predict through-focus visual acuity for pseudophakic patients." *Biomedical Optics Express* 7.5 (2016): 1877-1888.
- [32] Chae, S. H., Son, H. S., Khoramnia, R., Lee, K. H., & Choi, C. Y. (2020). Laboratory evaluation of the optical properties of two extended-depth-of-focus intraocular lenses. *BMC ophthalmology*, 20(1), 1-7.